RESULTS

TLX-Expressing Cells Are VZ-Specific Neural Stem Cells

Taking advantage of a β-galactosidase (β-gal) reporter that was knocked into the TLX loci, we examined the expression pattern of TLX in embryonic brains of TLX heterozygote mice. 5-Bromo-4-chloro-3-indolyl-β-galactopyranoside (X-gal) staining revealed that TLX is specifically expressed in the VZ of embryonic brains (Fig. 1A). Immunostaining with a β-gal-specific antibody showed similar VZ-specific staining pattern (Fig. 1B).

To examine more closely the expression pattern of TLX during mammalian neural development, a TLX-specific polyclonal antibody was developed. The specificity of the TLX antibody was revealed by both Western blot and immunofluorescence analyses. The TLX antibody detected a 46-kDa protein specifically in TLX stably transfected 3T3 cells (3T3-TLX), but not in parental 3T3 cells that have no endogenous TLX expression (Fig. 1C). Nuclear staining of TLX was also observed in 3T3-TLX cells specifically, but not in 3T3 cells. The TLX antibody also recognized endogenous TLX in neural stem cells and E14.5 brain lysates as revealed in Western blot analyses (Fig. 1C). Immunostaining of embryonic brain sections using the TLX-specific antibody revealed strong TLX expression in the periventricular zone of E14.5 wild-type and TLX heterozygous brains, whereas no staining was detected in the TLX-null brains (Fig. 1D). These results together indicate that TLX is specifically expressed in the germinal zone of embryonic brains.

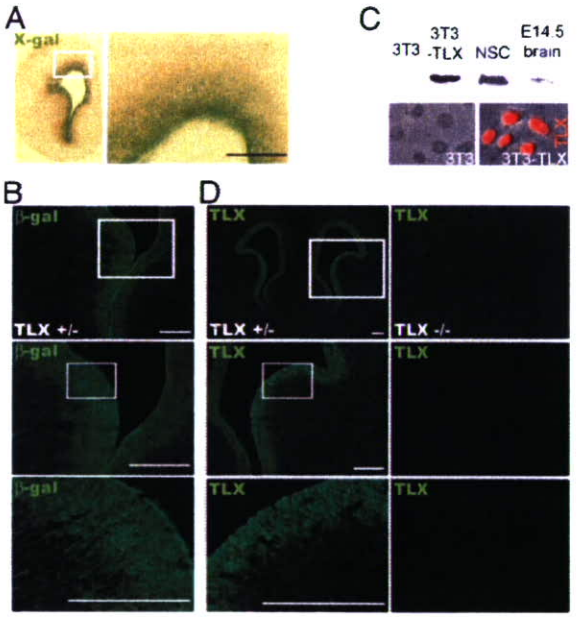

Fig. 1. Expression of TLX in the Ventricular Zone of E14.5 Brains

A, X-gal staining of β-gal enzymatic activity in coronal brain sections from E14.5 TLX+/− mice. B, Antibody staining of β-gal in brain sections from E14.5 TLX+/− mice. Enlarged images of the *boxed regions* were shown below the *boxed panels*. C, Characterization of TLX-specific antibody. Polyclonal antibody specific for TLX was generated against mouse TLX ligand-binding domain (amino acid residues 180–385). The *top panels* are Western blot analyses using cell lysates from 3T3, TLX-transfected 3T3 (3T3-TLX) cells, neural stem cells (NSC), and E14.5 brains. The *bottom panels* are immunofluorescence analysis of 3T3 and 3T3-TLX cells using the TLX antibody (shown in *red*). D, Immunostaining of coronal brain sections from E14.5 TLX+/− and TLX−/− mice. *Scale bar*, 200 μm. Enlarged images of the *boxed regions* are shown *below* the *boxed panels*.

To determine the identity of the TLX-expressing cells, we performed double immunostaining of embryonic brain sections using the TLX-specific antibody and antibodies specific to neural precursors or differentiated neurons. Previous studies suggested that nestin is a common marker of proliferating neural progenitors (15, 16). Immunohistological assessment of E14.5 brain sections from TLX+/− mice revealed colocalization of TLX and nestin in the VZ neural progenitor cells, with nuclear TLX staining and cytoplasm/process-specific nestin staining (Fig. 2A). Cortical neural progenitor cells are also marked by expression of RC2, a radial glial marker (17–19). Colocalization of

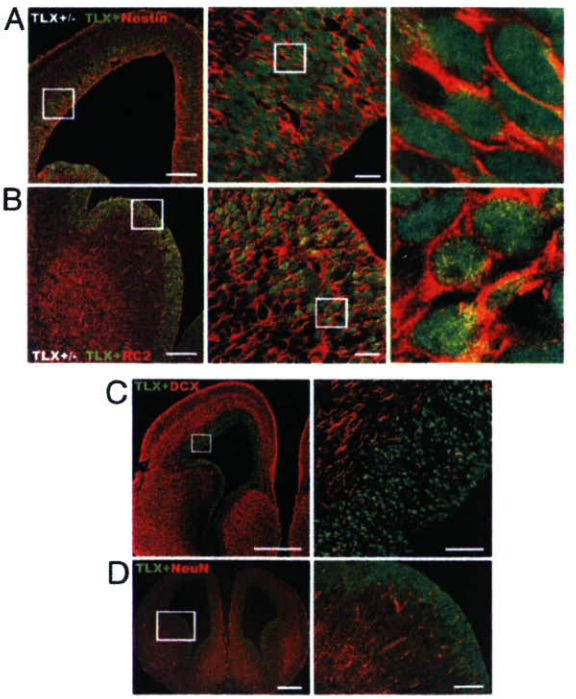

Fig. 2. TLX-Expressing Cells Are Nestin-Positive Embryonic Neural Precursor Cells

The TLX-expressing cells are nestin (A) and RC2 positive (B), but doublecortin (DCX, panel C) and NeuN (panel D) negative neural stem/progenitor cells in the VZ of mouse embryonic brains. The *boxed portions* are enlarged and shown in the *middle* and *right panels*. *Scale bars*: A (*left*), 200 μm; A (*middle*), 20 μm; scale bars in B are the same as in A; C (*left*), 500 μm; C (*right*), 50 μm; D (*left*), 400 μm; D (*right*), 100 μm.

TLX with RC2 (Fig. 2B) is evident throughout VZ, further supporting that TLX is expressed in embryonic neural precursor cells. In contrast, costaining of E14.5 brain sections with antibody specific to TLX and antibodies for neuronal markers doublecortin (DCX) or neuronal nuclei (NeuN) revealed distinct staining pattern of TLX and the neuronal markers (Fig. 2, C and D). The TLX-expressing cells are exclusively localized to the VZ, whereas DCX and NeuN-positive cells are specifically distributed to the intermediate zones and cortical plates. These results suggest that the TLX-expressing cells represent VZ-specific neural stem/progenitor cells in embryonic brains.

To further examine whether the TLX-expressing cells represent the actively dividing cells in the embryonic brains, we performed double staining of TLX and 5-bromodeoxyuridine (BrdU), a thymidine analog, on brain sections from TLX+/− E14.5 mice pretreated with BrdU. The analysis showed that TLX expression corresponds to both BrdU-positive and BrdU-negative cells in the embryonic brain germinal zone (Fig. 3A). In addition to BrdU labeling, which specifically marks cells at S phase, we also stained E14.5 brain sections with Ki67, a marker that labels all phases of the cell cycle, except the G0/G1 phase (20). Cells that are positive for both TLX and Ki67 staining were detected in the VZ of E14.5 brains (Fig. 3B). Because Ki67 labels a wider range of cells in the cell cycle, more cells were costained with TLX and Ki67 than costained with TLX and BrdU. A fraction of TLX-positive cells that are Ki67 negative was also detected in the VZ. These results suggest that TLX-expressing cells are primarily those actively dividing neural progenitors in cell cycle, but a small proportion could represent quiescent or nondividing cells in the VZ of embryonic brains.

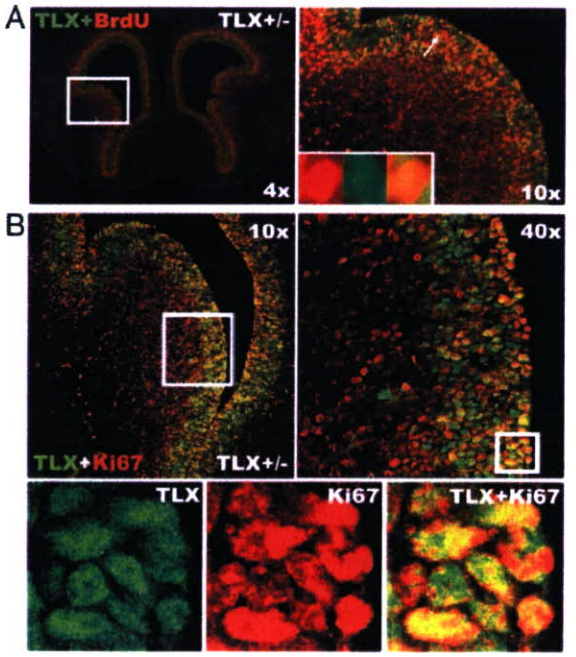

Fig. 3. Costaining of TLX and Proliferative Markers in Embryonic Brains

A, Costaining of TLX and BrdU. Brain sections from mice exposed to a single pulse of BrdU for 2 h before brain harvest were costained with antibodies specific to BrdU (*red*) and TLX (*green*). The *right panel* is the enlargement of the *boxed region* in the *left panel*. *Insets* in the *right panel* are enlarged images of the *arrow*-pointed cell shown in BrdU single staining (*red*), TLX single staining (*green*), and merged image of double staining. B, Costaining of TLX and Ki67. E14.5 brain sections were costained with antibodies specific for Ki67 (*red*) and TLX (*green*). The *right panel* (×40) is the enlargement of the *boxed region* in the *left panel* (×10). The *lower panels* are the enlargements of the *boxed region* in the ×40 image panel.

TLX Regulates Cell Cycle Progression in Embryonic Brains

To determine the role of TLX in embryonic brain development, we analyzed developing brains of TLX knockout mice. Serial Nissl staining of embryonic brains of TLX−/− mice at E14.5 revealed reduced areas of VZ and enlarged ventricles in TLX−/− brains, compared with that in wild-type brains (Fig. 4, A and B). The thinning of the VZ is more prominent in rostral sections than that in caudal sections, with the biggest differences in the ganglionic eminence of rostral sections (marked by *dotted lines* in panel 3).

The reduced areas of the VZ and the enlarged ventricles are probably due to the hypocellularity of the VZ. Therefore we determined whether there are decreased numbers of nestin-positive cells in the VZ of TLX−/− embryonic brains. Brain sections of wild-type and TLX−/− E14.5 embryos were immunostained with nestin-specific antibody. The number of nestin-positive cells was reduced in TLX−/− E14.5 brains (Fig. 4C, quantification in Fig. 4F), in good agreement with the reduced areas of VZ in TLX−/− embryonic brains (Fig. 4, A and B), suggesting that there are decreased numbers of neural precursors in the TLX−/− embryonic brains.

Programmed cell death (apoptosis) occurs during normal brain development (21). Increased cell death may contribute to reduced areas of VZ in TLX−/− embryonic brains. Apoptotic cell death was examined using terminal transferase dUTP nick end labeling (TUNEL) assay in wild-type and TLX−/− brains (Fig. 4D, quantification in Fig. 4G). Counts of total numbers of labeled cells revealed that cell death in transgenic brains was not substantially more than that found in wild-type mice, suggesting that the reduced neural stem/progenitor cells in TLX−/− embryonic brains did not result from increased apoptotic cell death.

Next we examined whether TLX affects cell proliferation in the embryonic brain. We used BrdU to label dividing neural precursor cells by exposing E14.5 embryos to BrdU for 2 h before brain harvest. Immunostaining of embryonic brain sections with BrdU-specific antibody was performed to monitor cell proliferation. Quantification of the BrdU-positive cells in both wild-type and TLX−/− E14.5 VZ revealed a significant decrease of total BrdU-positive cells in

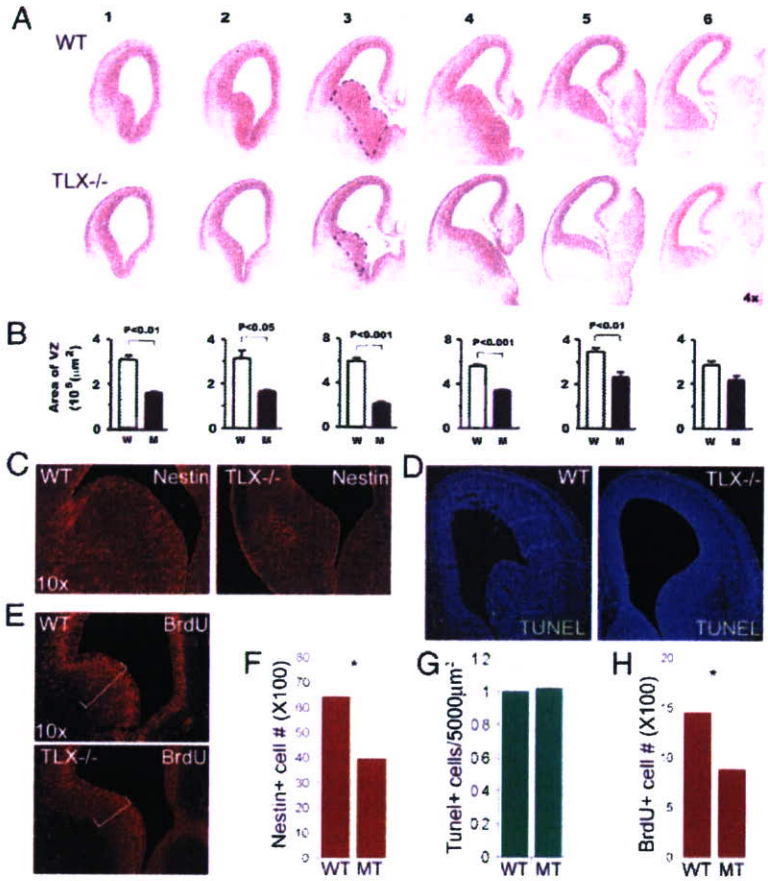

Fig. 4. Reduced Neural Progenitors and Cell Proliferation in E14.5 TLX−/− Brains

A, Nissl staining of coronal brain sections of E14.5 wild-type (WT) and mutant (MT) mice. The sections were divided into six matched panels from rostral to caudal. B, Quantification of the area of the lateral ganglionic eminence of VZ in each section shown in panel A, *P* value is indicated for statistical significance. C, Reduced neural progenitor cells in TLX−/− E14.5 brains as revealed by nestin immunostaining (*red*) of E14.5 wild-type and TLX−/− brains. D, No significant increase of apoptotic cell death in TLX−/− E14.5 brains. TUNEL assay of apoptosis (shown in *green*) in WT and TLX−/− E14.5 brains. DNA is counterstained with Hoechst 33342 (*blue*). E, Decreased cell proliferation in TLX−/− E14.5 brains as revealed by BrdU immunostaining (*red*) of brain sections from E14.5 wild-type and TLX−/− mice. F, Quantification of nestin-positive (nestin+) cells in WT and TLX−/− (MT) E14.5 VZ; *, $P < 0.01$. G, Quantification of TUNEL-positive cells in WT and TLX−/− (MT) E14.5 brains. H, Quantification of BrdU-positive (BrdU+) cells in WT and TLX−/− (MT) E14.5 VZ; *, $P < 0.01$.

TLX−/− brains, compared with wild-type brains (Fig. 4E, quantification in Fig. 4H). These results suggest that TLX plays a role in maintaining at least a subset of proliferative neural precursors in embryonic brains.

To examine whether the reduced cell proliferation in TLX−/− embryonic brains resulted from decreased mitotic rates, neural progenitor cells were labeled by a 30-min pulse of BrdU in E14.5 brains. The fraction of progenitor cells in S phase, a labeling index, was determined by scoring the percentage of BrdU-labeled neural progenitor cells (22). Progenitor cells were identified by Ki67 immunoreactivity (23, 24). Because the length of S phase remains relatively constant whereas the length of G1 phase regulates proliferation in mammalian cells (25), this labeling index provides an estimation of cell cycle length. If the cell cycle is lengthened, the relative fraction of cells labeled by a brief BrdU pulse would decrease. Examination of random fields chosen from eight brains (four wild-type and four mutant brains) revealed that the TLX−/− neural progenitor cells divided slower than did wild-type neural progenitors (Fig. 5A, quantification in Fig. 5C).

To determine whether the decrease in the number of VZ progenitor cells resulted from a reduction in the fraction of progenitor cells that remained undifferentiated, we examined cell cycle exit and reentry by scoring the fraction of cells dividing after pulse labeling with BrdU for 24 h before brain harvest. Cells that had left the cell cycle were identified as BrdU+ and Ki67−, and cells that remained in the cell cycle as BrdU+ and Ki67+. At E15.5, there was about a 2-fold decrease in the proportion of TLX mutant precursors that reentered the cell cycle when compared with wild-type neural precursors (Fig. 5B, quantification in Fig. 5D). These studies suggest that TLX functions in embryonic neural precursors to influence the decision of

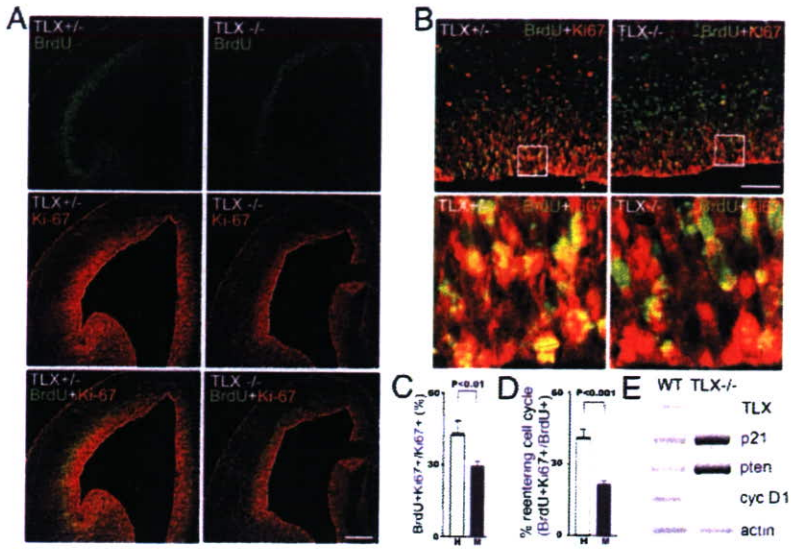

Fig. 5. TLX Regulates Cell Cycle Progression

A, Increased cell cycle length in E14.5. TLX−/− brains as revealed by decreased progenitor BrdU labeling index. The percentage of progenitor cells (Ki67, *red*) labeled with BrdU (*green*) after a 30-min BrdU pulse (BrdU+Ki67+/Ki67+) is reduced in TLX mutant brains. *Scale bar*, 200 μm. B, Reduced fraction of cells reentering cell cycles in E14.5 TLX−/− brains. Animals were exposed to a single pulse of BrdU 24 h before being killed; sections were stained with antibodies to BrdU (*green*) and Ki67 (*red*). Fraction of cells reentered cell cycle is calculated as BrdU+Ki67+ cells (cell reentered cell cycle)/ BrdU+Ki67+ cells plus BrdU+Ki67− cells (cells left cell cycle). More cells have left cell cycle in the mutant than in wild-type brains. *Scale bar*, 50 μm. C, Quantification of the percent of BrdU+Ki67+ cells out of Ki67+ cells in E14.5 TLX+/− (H) and TLX−/− (M) brains shown in panel A; $P < 0.01$ by Student's *t* test. D, Quantification of fraction of BrdU+Ki67+ cells out of BrdU+ cells in E14.5 TLX+/− (H) and TLX−/− (M) brains shown in panel B; $P < 0.001$ by Student's *t* test. E, RT-PCR analysis of gene expression in wild type (WT) and TLX−/− E14.5 brains. Cyc D1, Cyclin D1.

these cells to reenter the cell cycle instead of exiting cell cycle and becoming differentiated.

What is the molecular basis of TLX-mediated cell cycle regulation? To determine whether cell cycle-related genes are regulated by TLX in embryonic brains, mRNAs were isolated from E14.5 wild-type and from TLX−/− telencephelons, and RT-PCR analyses were performed. As shown in Fig. 5E, the expression of both the cyclin-dependent kinase inhibitor p21 and the tumor suppressor gene pten was up-regulated significantly in E14.5 TLX−/− telencephelons, suggesting that TLX represses both p21 and pten gene expression in embryonic brains. In addition, reduced expression of cyclin D1, a downstream effector of pten (26), was also detected. The up-regulation of a negative cell cycle regulator, p21, and the down-regulation of a positive cell cycle regulator, cyclin D1, provides a molecular mechanism for TLX-regulated cell cycle progression in the germinal zone of embryonic brains.

Transient Knockdown of TLX Led to Outward Migration of VZ Cells in Embryonic Brains

The relatively mild defect in TLX−/− embryonic brains, compared with the much more dramatic defect in TLX−/− adult brains (4), could be due to a systematic compensatory effect in embryonic stage to ensure proper development or redundant molecules that play overlapping roles in embryonic neural precursors. To further explore TLX function in embryonic brains with minimal systemic compensatory effect that could be caused by the systematic TLX knockout, a transient local knockdown approach was used by *in utero* electroporation (27–29), in which plasmid DNAs expressing TLX siRNAs were delivered directly into the VZ of intact embryos. Five TLX sequence-specific siRNAs were screened for the knockdown effect *in vitro*. Among the siRNAs tested, siRNA 2 had the strongest inhibitory effect on TLX expression (Fig. 6, A and B) and was therefore chosen for the subsequent electroporation-based *in vivo* studies. TLX siRNA-expressing DNA was introduced into cerebral cortices through *in utero* electroporation at E13.5, at a time when TLX expression is known to be high (3). Electroporated brains were dissected out and sectioned for analyses at E15.5. Cells that had taken up the siRNAs were labeled green by expression of green fluorescent protein (GFP) that was included in the vector and thus could be readily visualized by fluorescence microscopy. Electroporation of TLX siRNA led to a significant increase in the number of cells that migrate from VZ into intermediate zone and cortical plate 2 d after transfection, compared with that resulting from the transfection with control GFP vector (Fig. 6, C and D). The effectiveness of *in utero* siRNA knockdown was confirmed by TLX immunohistochemistry on brain sections from *in utero* electroporated embryos. Expression of TLX

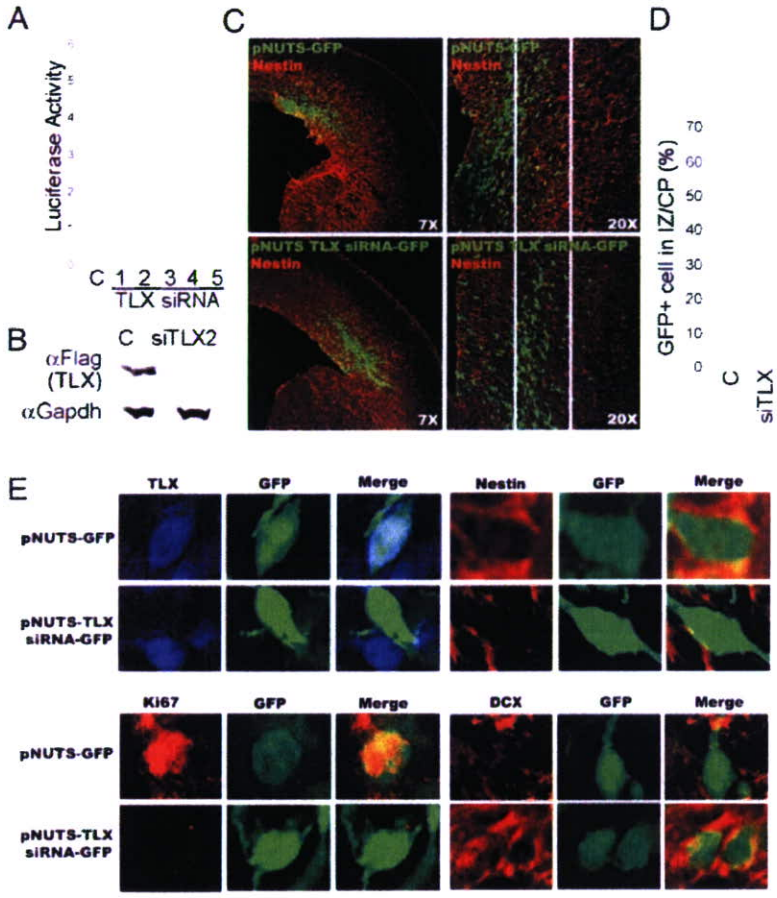

Fig. 6. *In Utero* Electroporation of TLX siRNA in Embryonic Brains

A, Luciferase assays to determine the repression effect of TLX siRNAs (1–5) using a luciferase reporter gene upstream of TLX coding sequences, compared with control GFP siRNA (C). Results represent the means and SDs of three replicates. B, siRNA knockdown of TLX expression in Flag-tagged TLX-transfected human embryonic kidney 293 cells as revealed by Western blot analysis. C, Control GFP siRNA; siTLX2: TLX siRNA 2. Anti-Flag antibody (αFlag) detects the Flag-tagged TLX. Gapdh was included as a loading control. C, pNUTS-GFP or pNUTS-TLX siRNA-GFP was introduced into E13.5 wild-type brains through *in utero* electroporation. Brains were dissected out at E15.5 for analyses. Cells that had taken up the transfected DNAs were shown *green* due to expression of a GFP marker. D, Quantification of control vector (C) and TLX siRNA-expressing vector (siTLX)-electroporated cells (GFP+) in intermediate zone (IZ) and cortical plate (CP). E, Immunostaining of cells from pNUTS-GFP or pNUTS-TLX-siRNA-GFP *in utero* electroporated embryonic brain sections.

siRNA-GFP led to dramatic decrease of TLX expression as revealed by the significant loss of TLX immunostaining, whereas expression of the control GFP vector had no effect on TLX expression (Fig. 6E, *upper left panels*).

Another nuclear receptor, peroxisomal proliferator-activated receptor-γ (PPARγ), has also been shown to regulate embryonic neural stem cells (30). To determine whether PPARγ plays a similar role to that of TLX in neural development, an *in vivo* knockdown experiment was performed using PPARγ-specific siRNA electroporated into VZ of E13.5 brains. In contrast to TLX siRNA, the PPARγ-specific siRNA (30) did not induce significant migration of VZ cells away from the apical side of the ventricle (data not shown).

The outward migration of the cells affected by TLX siRNA suggested that knockdown of TLX expression in the VZ of embryonic brains could have caused neural stem/progenitor cells to exit cell cycle and differentiate into neurons, which then migrate outward. Alternatively, siRNA knockdown of TLX expression could have induced nondifferentiated neural precursor cells to migrate out. To determine the possible mechanisms of the TLX siRNA-mediated cell migration, immunostaining of sections of siRNA-electroporated brains was done to determine the identity of the transfected cells. The TLX siRNA-transfected cells that migrated out of VZ lost the neural progenitor marker nestin (Fig. 6E, *upper right six panels*) and the proliferative marker Ki67 (Fig. 6E, *lower left six panels*). Instead, these cells expressed the neuronal marker, DCX (Fig. 6E, *lower right six panels*), indicating cell cycle exit and neuronal differentiation. In contrast, the control GFP vector-transfected cells that remained in the VZ were both nestin positive and Ki67 positive and lacked DCX expression (Fig. 6E). These results reinforce

that TLX is an important regulator of embryonic neural stem cells by controlling their cell cycle progression and exit.

DISCUSSION

The data presented here indicate that TLX plays an important role in the regulation of cell cycle progression and exit of embryonic neural stem cells. TLX is specifically expressed in neural precursor cells in the germinal zones of embryonic brains. Lack of TLX function during development results in reduced cell proliferation and decreased numbers of nestin-positive neural progenitor cells in the VZ of E14.5 brains. Both lengthened cell cycles and reduced fraction of cells reentering cell cycle could account for the reduced proliferation of progenitor cells in E14.5 TLX−/− brains. The increased expression of a negative cell cycle regulator, p21, and decreased expression of a positive cell cycle regulator, cyclin D1, provide a molecular basis for the lengthened cell cycle progression and reduced cell proliferation in the VZ of TLX−/− embryonic brains.

What are the primary cellular functions exerted by TLX in neural development? TLX could be required in early neural progenitor cells to regulate proliferative divisions and prevent neurogenesis under normal conditions. In support of this hypothesis, our data show that both knockout and transient siRNA knockdown of TLX led to increased cell cycle exit and reduced cell proliferation. TLX could also act by regulating the types of divisions that progenitor cells make. Early progenitor cells expand by symmetric divisions establishing the surface area and number of radial units in the cortex (31). Subsequently, there is a steady increase in the number of differentiative asymmetric divisions, establishing the number of neurons per radial unit and the depth of the cerebral cortex. Therefore the length of the cell cycle and the duration of each phase of division are critical in controlling the size of the cerebral cortex (32–34). Our data suggest that progenitor cells in TLX-mutant animals go through fewer cell cycles than that in their wild-type littermates, perhaps by prematurely switching from symmetric divisions to asymmetric divisions. TLX has also been shown to be required to regulate the timing of neurogenesis in the cortex (35) and to control patterning of lateral telencephalic progenitor domains during development (36). The results presented here demonstrated unambiguously that TLX regulates cell cycle progression and exit to maintain embryonic neural stem cells in the undifferentiated and proliferative state through controlling key cell cycle regulator gene expression.

Interestingly, the defect in TLX mutant embryonic brains is modest compared with the dramatic deficiency in TLX-null adult brains. It is a surprise that there are still rigorous cell proliferation and extensive numbers of nestin-positive neural progenitor cells in the VZ of TLX-mutant embryonic brains, in contrast to almost complete loss of cell proliferation in TLX−/− adult brains (4). These results suggest that TLX may not be the sole regulator of neural stem cell maintenance during development. There could be other molecules that play redundant roles in neural stem cell regulation during embryogenesis. Alternatively, the organism could have a fail-safe mechanism to compensate for the systemic TLX loss to ensure proper development. To minimize the potential systemic compensatory effect, we took a transient local knockdown approach. Our observation that a significantly increased number of VZ cells underwent outward migration upon transient local TLX knockdown reinforces an important role of TLX in embryonic neural stem cells and supports the compensatory possibility. In contrast to siRNA knockdown of TLX, siRNA knockdown of another nuclear receptor, PPARγ, which is also expressed in embryonic brains and has been shown to play a role in embryonic neural stem cell regulation (30), did not cause migration of the transfected cells, suggesting that PPARγ plays a distinct role from TLX in embryonic neural stem cells.

The characterization of the TLX-expressing cells in the embryonic brain provides a means to elucidate the molecular and cellular mechanisms underlying embryonic neural stem cell proliferation and differentiation. Although other factors are likely involved, TLX is an important regulator of neural stem cells in the developing brain by regulating the expression of key cell cycle regulators.

MATERIALS AND METHODS

Experimental Animals

All research animals are acquired and used in compliance with federal, state, and local laws and institutional regulations. All animals are maintained in accordance with the NIH Guide for the Care and Use of Laboratory Animals. The studies were approved by the institutional committee on animal care.

Animal Handling and Brain Tissue Preparation

Strain-matched and age-matched mice were used in all experiments. All animal experiments were performed in compliance with institutional and NIH guidelines. TLX heterozygous male and female mice were used for breeding to obtain wild-type, TLX-heterozygous, and null embryos. Timed-pregnant mice were anesthetized with ketamine (120 mg/kg) and xylazine (10 mg/kg). Embryonic brains were dissected and fixed in 4% paraformaldehyde in 0.1 M PBS (pH 7.4) at 4 C overnight, and cryoprotected in 7.5%, 15%, and 30% sucrose in phosphate buffer at 4 C for 2 h, 2 h, and 24 h, respectively. After cryoprotection, brain tissues were embedded in OCT, frozen with dry ice, and stored at −80 C. Coronal sections of forebrains (12 μm) were cut on a cryostat and mounted onto superfrost-plus slides (Fisher Scientific, Pittsburgh, PA).

BrdU Labeling

For BrdU labeling, timed-pregnant mice were injected with 50 mg/kg BrdU (Sigma Chemical Co., St. Louis, MO) in saline ip. Animals were killed in 30 min (E14.5 injection), 2 h (E14.5 injection), or 24 h (E13.5 injection). Embryos were dissected and sectioned as described above. Brain sections were pretreated in 2 N HCl for 30 min at 37 C, followed by neutralization in 0.1 M

borate buffer (pH 8.5) for 10 min and blocking with 10% normal donkey serum for 1 h at room temperature, after which immunohistochemistry was performed using a rat anti-BrdU monoclonal antibody (1:300, Accurate) and donkey antirat fluorescein isothiocyanate or cyanine dye 3-conjugated secondary antibody (1:300, Jackson ImmunoResearch Laboratories, Inc., West Grove, PA). BrdU immunostaining was observed using a Nikon Eclipse fluorescent microscope (TE2000-S) and imaged using Spot Camera (version 4.0.8, Diagnostic Instruments, Sterling Heights, MI). The number of BrdU-positive cells was counted in the area of the lateral ventricle zones of E14.5 brains with a minimum of six sections per embryo from five wild-type and five mutant embryos. Cell densities were calculated by dividing cell numbers by the area. Student's *t* test was used to determine the *P* value for statistical significance. All comparisons were made between littermates.

Immunohistochemistry, Nissl Staining, and LacZ Staining

Brain coronal sections (12 μm) from the same litter were used for Nissl staining. The forebrain sections were divided into six matched patterns from rostral to caudal between TLX mutant mice and their littermate wild-type controls. Statistical analysis was performed with Student's *t* test. For X-gal staining, embryos were fixed in 4% paraformaldehyde in 0.1 M PBS (pH 7.4) for 3 h, the 40-um frozen sections were fixed with glutaraldehyde and paraformaldehyde and stained in (X-gal; Life Technologies, Inc., Gaithersburg, MD) solution containing 20 mM K-ferricyanide, 20 mM K-ferrocyanide, 0.01% sodium deoxycholate, 0.02% Nonidet P-40, and 2 mM $MgCl_2$. For immunohistochemistry, 12-μm brain sections were incubated with antibodies, including mouse antinestin (1:1,000, PharMingen, San Diego, CA), mouse anti-RC2 (1:30, Hybridoma Bank), rabbit anti-TLX (1:100, Shi laboratory), goat anti-DCX (1:100, Santa Cruz Biotechnology, Inc., Santa Cruz, CA), mouse anti-NeuN (1:1000; Chemicon, Temecula, CA), rabbit anti-Tuj1 (1:4000; Covance Laboratories, Inc., Madison, WI), guinea pig anti-GFAP (1:500, Advanced Immunochemical Inc., Long Beach, CA), rabbit anti-β-gal (1:3500, Cortex Biochem, Inc., San Leandro, CA), rabbit anti-Ki67 (Novocastra Laboratories, Newcastle, UK; 1:100), mouse anti-Ki67 (Novocastra; 1:40), followed by incubation with cyanine dye 3 or fluorescein isothiocyanate-conjugated secondary antibodies (1:400, Jackson ImmunoResearch). Images were visualized by a confocal microscope (Zeiss LSM510 Upright 2 photon; Carl Zeiss, Thornwood, NY). Quantitative studies were based on four or more replicates. Nestin-positive cells were counted within the region of the lateral ganglionic eminence in E14.5 brains of nine wild-type and six TLX−/− embryos. Student's *t* test was used to determine the *P* value for statistical significance. All comparisons were made between littermates.

TLX Polyclonal Antibody Production, Western Blot, and Immunofluorescence

The TLX antigen containing mouse TLX ligand binding domain (amino acid residues 180–385) was produced in bacteria BL21 cells as His-tagged protein and purified using Ni-NTA Agarose (QIAGEN, Hilden, Germany). Rabbit immunizations were performed in the Animal Resource Center in City of Hope. The anti-TLX serum was further purified using SulfoLink Coupling Gel (Pierce Biotechnology, Inc., Rockford, IL). For Western blot, TLX antibody was used at 1:1000 dilution; for immunofluorescence on 3T3 or 3T3-TLX cells, TLX antibody was also used at 1:1000 dilution.

In Utero Electroporation

TLX or PPARγ siRNAs were cloned into pNUTs-GFP, a mouse U6 promoter-based small RNA-expressing vector that contains an ubiquitin promoter-driven enhanced GFP (a gift from David Baltimore, Caltech). pNUTs-GFP, pNUTs-GFP-TLX siRNA, and pNUTs-GFP-PPARγ siRNA vectors were used in *in utero* electroporation analyses. The plasmids were prepared at 5 μg/μl in H_2O with either QIAGEN HighSpeed plasmid maxi kit (QIAGEN) or NucleoBond plasmid purification maxi kit (CLONTECH Laboratories, Inc., Palo Alto, CA). The plasmids have the GFP reporter gene downstream of an Ubiquitin promoter (pNUTS). For *in utero* electroporation, mice at 12.5-d gestation were anesthetized with an ip injection of ketamine (120 mg/kg) and xylazine (10 mg/kg). The uterine horns were exposed, and 1 μl plasmid DNA (5 μg/μl) was microinjected by pressure using picospritzer III (General valve operation, Fairfield, NJ) through the uterus into the lateral ventricles of embryos by pulled glass capillaries (Drummond Scientific Co., Broomall, PA). Electroporation was accomplished by holding the injected brain through the uterus with forcep-type electrodes CY650-P5 (Protech International, Inc., San Antonio, TX) and delivering square electric pulses (five pulses; duration, 50 msec each; interval, 950 msec) to the embryos using electroporator CUY-21 (Protech International). The mice are allowed to survive 2 d before being euthanized. Brains of embryos were harvested and analyzed.

RT-PCR Analysis

Total RNA was isolated using Trizol reagent (Life Technologies, Inc.). For RT-PCR analysis, reverse transcription was performed using Omniscript RT kit (QIAGEN). PCR primers used were TCT CTA TGT TCC AAA ACC ATT CCA T and TTC CCA AGC ACC TCA TAC TAC CAG C for cyclin D1, ATA TCC AGA CAT TCA GAG CCA CAG G and GGA AAC ACA GAG CTT GGG TTG GGA G for p21, GCT ACC AGA CTC TCA CAG GAG CAA GC and TCA GAC TTT TGT AAT TTG TGA ATG CT for pten, and TCT TCA CCA CCA TGG AGA AGG C and CTG ACA ATC TTG AGT GAG TTG T for actin.

Luciferase Assay

TLX siRNA sequences were cloned into the pCSC vector (4). The reporter vector was constructed by insertion of the TLX coding region into the sicheck 2.2 vector (Promega) downstream of the *Renilla* luciferase reporter gene. Quantities of 0.64 μg TLX siRNA expressing plasmids, 0.08 μg sicheck reporter construct, and 2 μl Fugene 6 (Roche Clinical Laboratories, Indianapolis, IN) were mixed in 500 μl of cell culture media, incubated at room temperature for 20 min, and added dropwise to three wells of human embryonic kidney 293 cells in 48-well plates. Reporter *Renilla* luciferase activity and internal control firefly luciferase activity were measured 48 h after transfection using Dual Luciferase Assay kit (Promega). The reporter luciferase activity was normalized with the internal control for transfection efficiency and plotted on the y-axis.

Acknowledgments

We thank Drs. Kamil Alzayady, Qiang Lu, Paul Salvaterra, Toshi Tomoda, and John Zaia for critical reading of the manuscript, and Dr. Smitha Reddy Anam for technical help.

Received June 12, 2007. Accepted September 18, 2007.

Address all correspondence and requests for reprints to: Yanhong Shi, Neuroscience Division, Beckman Research Institute of City of Hope, 1500 East Duarte Road, Duarte, California 91010. E-mail: yshi@coh.org.

This work was supported by Whitehall Foundation, the Margret E. Early Medical Trust, and National Institutes of Health National Institute of Neurological Diseases and Stroke Grants R01NS059546 and R21NS 053350. G.S. is a Herbert Horvitz Postdoctoral Fellow. Y.S. is a Kimmel Scholar.

Disclosure Statement: The authors have nothing to disclose.

REFERENCES

1. Evans RM 2005 The nuclear receptor superfamily: a rosetta stone for physiology. Mol Endocrinol 19:1429–1438
2. Yu RT, McKeown M, Evans RM, Umesono K 1994 Relationship between *Drosophila* gap gene tailless and a vertebrate nuclear receptor Tlx. Nature 370:375–379
3. Monaghan AP, Grau E, Bock D, Schutz G 1995 The mouse homolog of the orphan nuclear receptor tailless is expressed in the developing forebrain. Development 121: 839–853
4. Shi Y, Chichung Lie D, Taupin P, Nakashima K, Ray J, Yu RT, Gage FH, Evans RM 2004 Expression and function of orphan nuclear receptor TLX in adult neural stem cells. Nature 427:78–83
5. Monaghan AP, Bock D, Gass P, Schwager A, Wolfer DP, Lipp HP, Schutz G 1997 Defective limbic system in mice lacking the tailless gene. Nature 390:515–517
6. Chiang MY, Evans RM 1997 Reverse genetic analysis of nuclear receptors, RXRg, RARb, and TLX in mice, PhD dissertation, University of California San Diego
7. Roy K, Thiels E, Monaghan AP 2002 Loss of the tailless gene affects forebrain development and emotional behavior. Physiol Behav 77:595–600
8. Young KA, Berry ML, Mahaffey CL, Saionz JR, Hawes NL, Chang B, Zheng QY, Smith RS, Bronson RT, Nelson RJ, Simpson EM 2002 Fierce: a new mouse deletion of Nr2e1; violent behaviour and ocular abnormalities are background-dependent. Behav Brain Res 132:145–158
9. Yu RT, Chiang MY, Tanabe T, Kobayashi M, Yasuda K, Evans RM, Umesono K 2000 The orphan nuclear receptor Tlx regulates Pax2 and is essential for vision. Proc Natl Acad Sci USA 97:2621–2625
10. Miyawaki T, Uemura A, Dezawa M, Yu RT, Ide C, Nishikawa S, Honda Y, Tanabe Y, Tanabe T 2004 Tlx, an orphan nuclear receptor, regulates cell numbers and astrocyte development in the developing retina. J Neurosci 24:8124–8134
11. Uemura A, Kusuhara S, Wiegand SJ, Yu RT, Nishikawa S 2006 Tlx acts as a proangiogenic switch by regulating extracellular assembly of fibronectin matrices in retinal astrocytes. J Clin Invest 116:369–377
12. Zhang CL, Zou Y, Yu RT, Gage FH, Evans RM 2006 Nuclear receptor TLX prevents retinal dystrophy and recruits the corepressor atrophin1. Genes Dev 20:1308–1320
13. Abrahams BS, Mak GM, Berry ML, Palmquist DL, Saionz JR, Tay A, Tan YH, Brenner S, Simpson EM, Venkatesh B 2002 Novel vertebrate genes and putative regulatory elements identified at kidney disease and NR2E1/fierce loci. Genomics 80:45–53
14. Abrahams BS, Kwok MC, Trinh E, Budaghzadeh S, Hossain SM, Simpson EM 2005 Pathological aggression in "fierce" mice corrected by human nuclear receptor 2E1. J Neurosci 25:6263–6270
15. Lendahl U, Zimmerman LB, McKay RD 1990 CNS stem cells express a new class of intermediate filament protein. Cell 60:585–595
16. Reynolds BA, Tetzlaff W, Weiss S 1992 A multipotent EGF-responsive striatal embryonic progenitor cell produces neurons and astrocytes. J Neurosci 12:4565–4574
17. Malatesta P, Hartfuss E, Gotz M 2000 Isolation of radial glial cells by fluorescent-activated cell sorting reveals a neuronal lineage. Development 127:5253–5263
18. Miyata T, Kawaguchi A, Okano H, Ogawa M 2001 Asymmetric inheritance of radial glial fibers by cortical neurons. Neuron 31:727–741
19. Noctor SC, Flint AC, Weissman TA, Dammerman RS, Kriegstein AR 2001 Neurons derived from radial glial cells establish radial units in neocortex. Nature 409:714–720
20. Schluter C, Duchrow M, Wohlenberg C, Becker MH, Key G, Flad HD, Gerdes J 1993 The cell proliferation-associated antigen of antibody Ki-67: a very large, ubiquitous nuclear protein with numerous repeated elements, representing a new kind of cell cycle-maintaining proteins. J Cell Biol 123:513–522
21. Kuan CY, Roth KA, Flavell RA, Rakic P 2000 Mechanisms of programmed cell death in the developing brain. Trends Neurosci 23:291–297
22. Chenn A, Walsh CA 2002 Regulation of cerebral cortical size by control of cell cycle exit in neural precursors. Science 297:365–369
23. Scholzen T, Gerdes J 2000 The Ki-67 protein: from the known and the unknown. J Cell Physiol 182:311–322
24. Kee N, Sivalingam S, Boonstra R, Wojtowicz JM 2002 The utility of Ki-67 and BrdU as proliferative markers of adult neurogenesis. J Neurosci Methods 115:97–105
25. DiSalvo CV, Zhang D, Jacobberger JW 1995 Regulation of NIH-3T3 cell G1 phase transit by serum during exponential growth. Cell Prolif 28:511–524
26. Weng LP, Brown JL, Eng C 2001 PTEN coordinates G(1) arrest by down-regulating cyclin D1 via its protein phosphatase activity and up-regulating p27 via its lipid phosphatase activity in a breast cancer model. Hum Mol Genet 10:599–604
27. Fukuchi-Shimogori T, Grove EA 2001 Neocortex patterning by the secreted signaling molecule FGF8. Science 294:1071–1074
28. Saito T, Nakatsuji N 2001 Efficient gene transfer into the embryonic mouse brain using in vivo electroporation. Dev Biol 240:237–246
29. Tabata H, Nakajima K 2001 Efficient in utero gene transfer system to the developing mouse brain using electroporation: visualization of neuronal migration in the developing cortex. Neuroscience 103:865–872
30. Wada K, Nakajima A, Katayama K, Kudo C, Shibuya A, Kubota N, Terauchi Y, Tachibana M, Miyoshi H, Kamisaki Y, Mayumi T, Kadowaki T, Blumberg RS 2006 Peroxisome proliferator-activated receptor γ-mediated regulation of neural stem cell proliferation and differentiation. J Biol Chem 281:12673–12681
31. Rakic P 1988 Specification of cerebral cortical areas. Science 241:170–176
32. Rakic P 1995 A small step for the cell, a giant leap for mankind: a hypothesis of neocortical expansion during evolution. Trends Neurosci 18:383–388
33. Takahashi T, Nowakowski RS, Caviness Jr VS 1996 The leaving or Q fraction of the murine cerebral proliferative epithelium: a general model of neocortical neuronogenesis. J Neurosci 16:6183–6196
34. Caviness Jr VS, Goto T, Tarui T, Takahashi T, Bhide PG, Nowakowski RS 2003 Cell output, cell cycle duration and neuronal specification: a model of integrated mechanisms of the neocortical proliferative process. Cereb Cortex 13:592–598
35. Roy K, Kuznicki K, Wu Q, Sun Z, Bock D, Schutz G, Vranich N, Monaghan AP 2004 The Tlx gene regulates the timing of neurogenesis in the cortex. J Neurosci 24:8333–8345
36. Stenman JM, Wang B, Campbell K 2003 Tlx controls proliferation and patterning of lateral telencephalic progenitor domains. J Neurosci 23:10568–10576

Molecular Endocrinology **is published monthly by The Endocrine Society (http://www.endo-society.org), the foremost professional society serving the endocrine community.**

MOLECULAR AND CELLULAR BIOLOGY, July 2007, p. 4931–4937 Vol. 27, No. 13
0270-7306/07/$08.00+0 doi:10.1128/MCB.02435-06

Potentiation of Astrogliogenesis by STAT3-Mediated Activation of Bone Morphogenetic Protein-Smad Signaling in Neural Stem Cells▽†

Shinji Fukuda,[1,2] Masahiko Abematsu,[3] Hiroyuki Mori,[4] Makoto Yanagisawa,[1,2]‡ Tetsushi Kagawa,[1,2] Kinichi Nakashima,[3] Akihiko Yoshimura,[4] and Tetsuya Taga[1,2]*

Department of Cell Fate Modulation, Institute of Molecular Embryology and Genetics,[1] and The 21st Century COE Program "Cell Fate Regulation Research and Education Unit,"[2] Kumamoto University, 2-2-1 Honjo, Kumamoto 860-0811, Laboratory of Molecular Neuroscience, Graduate School of Biological Sciences, Nara Institute of Science and Technology, 8916-5 Takayama, Ikoma 630-0101,[3] and Division of Molecular and Cellular Immunology, Medical Institute of Bioregulation, Kyushu University, 3-1-1 Maidashi, Higashi-ku, Fukuoka 812-8582,[4] Japan

Received 30 December 2006/Returned for modification 21 February 2007/Accepted 10 April 2007

Astrocytes play important roles in brain development and injury response. Transcription factors STAT3 and Smad1, activated by leukemia inhibitory factor (LIF) and bone morphogenetic protein 2 (BMP2), respectively, form a complex with the coactivator p300 to synergistically induce astrocytes from neuroepithelial cells (NECs) (K. Nakashima, M. Yanagisawa, H. Arakawa, N. Kimura, T. Hisatsune, M. Kawabata, K. Miyazono, and T. Taga, Science 284:479–482, 1999). However, the mechanisms that govern astrogliogenesis during the determination of the fate of neural stem cells remain elusive. Here we found that LIF induces expression of BMP2 via STAT3 activation and leads to the consequent activation of Smad1 to efficiently promote astrogliogenic differentiation of NECs. The BMP antagonist Noggin abrogated LIF-induced Smad1 activation and astrogliogenesis by inhibiting BMPs produced by NECs. NECs deficient in suppressor of cytokine signaling 3 (SOCS3), a negative regulator of STAT3, readily differentiated into astrocytes upon activation by LIF not only due to sustained activation of STAT3 but also because of the consequent activation of Smad1. Our study suggests a novel LIF-triggered positive regulatory loop that enhances astrogliogenesis.

Astrocytes are not only a structural component of the central nervous system (CNS) (7) but also important participants in the generation and regeneration of the CNS, for instance, in the regulation of synaptic formation, neurotransmitter transport, metabolic functions, and the response to CNS injury (7). A recent study showed that glial fibrillary acidic protein (GFAP)-positive reactive astrocytes contribute to tissue repair and motor function restoration during the subacute phase of CNS injury by forming glial scars (25). Astrocytes arise from neural stem cells that also produce neurons and oligodendrocytes. Cytokines and growth factors play critical roles in the cell fate specification of neural stem cells (31). Neuroepithelial cells (NECs) isolated from mouse embryonic telencephalons are rich in neural stem cells. Differentiation of NECs into GFAP-positive mature astrocytes is induced by interleukin 6 (IL-6) family cytokines (e.g., leukemia inhibitory factor [LIF] and ciliary neurotrophic factor) and bone morphogenetic protein (BMP) family cytokines (e.g., BMP2 and BMP4) (2, 8), which activate distinct downstream transcription factors, STAT3 and Smad1 (or Smad5 or Smad8), respectively (17, 36). A molecular basis for the cooperative action of these two cytokines is suggested to be the formation of a STAT3-Smad1 complex with a coactivator, p300, that initiates astrocyte-specific gene expression (21, 22). Significant reductions in the levels of GFAP-positive astrocytes were observed in mice deficient in gp130, a STAT3-upstream signal-transducing receptor component for IL-6 family cytokines (20), and in NECs overexpressing Noggin, a BMP antagonist that inhibits Smad1 signaling (33). These results indicate the importance of cross talk between STAT3 and Smad1 signaling pathways in astrogliogenesis, but the molecular mechanisms that govern astrogliogenesis are still largely unknown.

In an attempt to identify molecules crucial for the regulation of cytokine-mediated astrogliogenesis, we prepared NECs from embryonic day 14.5 (E14.5) mice and used DNA microarray analysis to compare the gene expression profiles under culture conditions with and without LIF and BMP2, an astrogliogenic combination of cytokines. Genes whose expression was upregulated in response to LIF plus BMP2 included glial cell lineage-related genes (STAT3, CD44, and AMOG [9, 15, 26]) and previously reported cytokine response genes in neural precursor cells (Id1, Id3, c-*fos*, C/EBPδ, suppressor of cytokine signaling 2 [SOCS2], and SOCS3 [4, 19, 39, 41]). Since SOCS3 is known as a negative regulator of the LIF-downstream transcription factor STAT3, we focused on SOCS3.

Members of the SOCS family of proteins are known as cytokine-inducible factors that negatively regulate the JAK-STAT pathway (14). Representatives of the SOCS family SOCS1, SOCS2, and SOCS3 have a centrally located SH2 domain and a C-terminal SOCS box as their common feature. Cytokine-induced SOCS proteins interact with their upstream receptors and inhibit the activation of relevant members of the STAT family of transcription factors, which attenuate signal

* Corresponding author. Mailing address: Department of Cell Fate Modulation, Institute of Molecular Embryology and Genetics, Kumamoto University, 2-2-1 Honjo, Kumamoto 860-0811, Japan. Phone: 81-96-373-6610. Fax: 81-96-373-6614. E-mail: taga@kumamoto-u.ac.jp.

† Supplemental material for this article may be found at http://mcb.asm.org/.

‡ Present address: Institute of Molecular Medicine and Genetics, Medical College of Georgia, 1120 15th Street, Augusta, GA 30912.

▽ Published ahead of print on 23 April 2007.

transduction, thereby establishing negative feedback loops in the cytokine response. In the present study, experiments on the function of SOCS3 in NECs provided us with a clue to identify a previously unsuspected signal-modifying mechanism governing astrogliogenesis: LIF induces expression of its cooperative partner cytokine in astrocyte differentiation, i.e., BMP2, and leads to consequent Smad1 activation to efficiently form the astrogliogenic transcription factor complex.

MATERIALS AND METHODS

Animals, cell culture, and cytokines. The *Socs3* gene was conditionally deleted by Cre recombinase expressed under the control of the nestin gene promoter (18). For experiments comparing the properties of wild-type cells with those of SOCS3-deficient cells, littermates were first obtained by crossing Nes-*cre*$Socs3^{flox/flox}$ mice (with a conditional knockout regulated by nestin expression) and $Socs3^{flox/flox}$ mice (wild type) and then genotyped according to a previous report (18). Mice were treated according to the guidelines of the Center for Animal Resources and Development, Kumamoto University. NECs were isolated from the telencephala of E14.5 mice and cultured for 4 days in N2-supplemented Dulbecco's modified Eagle medium–F-12 containing FGF2 (10 ng/ml) as described previously (21). SOCS3-deficient mouse embryonic fibroblasts (MEFs) were maintained as described previously (16). Cytokines were obtained from the following companies: FGF2 from Peprotech, LIF (ESGRO) from Invitrogen, and BMP4 and Noggin/Fc chimera from R&D Systems. BMP2 was kindly provided by Astellas Pharma Inc.

DNA microarray analysis. The Affymetrix GeneChip system was used to identify cytokine response genes. NECs, maintained as described above, were detached and replated on 10-cm-diameter dishes (1.5×10^7 cells/dish). On the following day, cells were treated with both LIF and BMP2 (80 ng/ml each) for 6 h. NECs cultured in the absence of the cytokines were used as a control. Probes were prepared using 3.5 μg of purified poly(A) RNA and were hybridized with murine genome U74Av2 arrays according to the recommended protocol. After the hybridization, DNA chips were processed by the fluidics station and scanner. Affymetrix Microarray Suite 5.0 was used to compare the gene expression profiles of cytokine-treated NECs with those of untreated cells. DNA microarray data are available upon request.

Expression plasmids and RT-PCR analysis. The cDNA for mouse SOCS3 was obtained by reverse transcription-PCR (RT-PCR) using the oligonucleotides listed below as described previously (6) and was cloned into the pcDNA3.1 expression vector (Invitrogen). Other expression plasmids are described in our previous reports (6, 21). Semiquantitative PCR was performed using KOD-plus (Toyobo) or Phusion (Finzymes) DNA polymerase. Primer sequences used for RT-PCR are as follows: SOCS3-F, 5′-CCGGAATTCATGGTCACCCACAGC AAGTT-3′; SOCS3-R, 5′-TGCTCTAGATTAAAGTGGAGCATCATACT-3′; BMP2-F, 5′-AGAGATGAGTGGGAAAACGG-3′; BMP2-R, 5′-GAAGTCCA CATACAAAGGGT-3′; GAPDH-F, 5′-ACCACAGTCCATGCCATCAC-3′; GAPDH-R, 5′-TCCACCACCCTGTTGCTGTA-3′.

Luciferase assay. NECs replated on 12-well plates were transfected using TransIT-LT1 (Mirus) as described previously (21). MEFs were transfected using Lipofectamine 2000 (Invitrogen) according to the manufacturer's protocol. On the day following the transfection, cells were treated with BMP2, BMP4, or LIF (50 ng/ml) for 8 h. The GFAP promoter-luciferase reporter plasmid, GF1L-pGL3, is described in our previous report (21). 4xB2wt-pGL3 and 4xB2mut-pGL3 were made by subcloning two oligonucleotide repeats (wild-type, 5′-TCG ACATCC**TTCAGAGAA**TTCTGATCC**TTCAGAGAA**TTCTGGGTAC-3′; mutant, 5′-TCGACATCC**CCAAGAGAA**TTCTGATCC**CCAAGAGAA**TTCTGGGTAC-3′; mutations are underlined) in front of the *junB* minimal promoter with the luciferase gene as described previously (37). These oligonucleotides contain two repeats of a potential STAT3 binding site identified in the 5′ region of the mouse *Bmp2* gene (boldfaced) and additional SalI and KpnI sites at each end. As an internal control, pEF-Rluc (21) or phRL-TK (Promega) was used.

Antibodies and Western blot analysis. The following antibodies were used in this study: anti-SOCS3 (1:50; catalog no. 18391; Immuno-Biological Laboratories), anti-GFP (1:200 [catalog no. G6539; Sigma] and 1:500 [catalog no. 598; MBL]), anti-GFAP (1:500 [catalog no. G3893; Sigma] and 1:1,000 [catalog no. 031223; Advanced ImmunoChemical]), nestin (1:1,000; catalog no. 556309; BD Pharmingen), anti-phospho-STAT3 Tyr705 (1:500; catalog no. 9131; Cell Signaling), anti-STAT3 (1:1,000; catalog no. sc482; Santa Cruz), anti-phospho-ERK1/2 Thr202/Tyr204 (1:500; catalog no. 9106; Cell Signaling), anti-ERK1 (1:1,000; catalog no. sc93; Santa Cruz), anti-ERK2 (1:1,000; catalog no. sc154; Santa Cruz), anti-phospho-Smad1 Ser463/465 (1:200 for immunocytochemistry and 1:500 for Western blot analysis; catalog no. 06-702; Upstate), and anti-Smad1 (1:1,000; catalog no. sc7153; Santa Cruz). Western blot analysis was performed as described previously (6). For the repeated reprobing in Western blotting, WB stripping solution (Nacalai Tesque) was used.

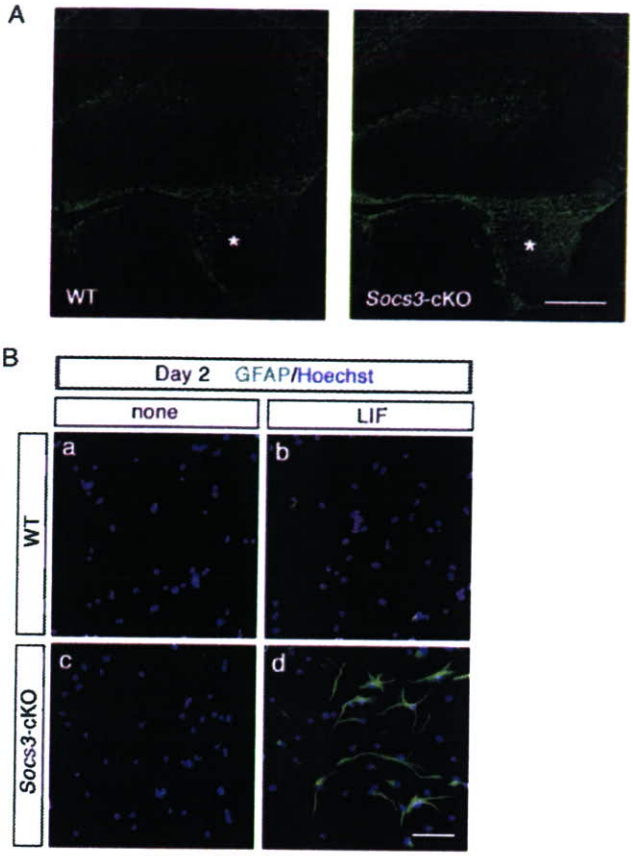

FIG. 1. SOCS3-deficient NECs readily differentiate into astrocytes upon induction by LIF. (A) Enhanced astrogliogenesis in the SOCS3-deficient neonatal mouse brain. Immunohistochemical analysis of GFAP expression was performed using cryosection of wild-type and *Socs3*-cKO mice at P1.5. Asterisks indicate fimbriae. Bar, 500 μm. (B) NECs derived from wild-type and *Socs3*-cKO mice were cultured in the absence (a and c) or presence (b and d) of LIF (80 ng/ml) for 2 days. Cells were fixed and stained with an anti-GFAP antibody (green). Nuclei were stained with Hoechst 33258 (blue). Bar, 50 μm.

Immunostaining. For immunocytochemistry, NECs expanded in the presence of FGF2 were counted and replated on the appropriate culture dishes or chamber slides. Six hours later, cytokines (LIF, 80 ng/ml; Noggin, 200 ng/ml) were added as indicated. After the incubation, cells were fixed in 4% paraformaldehyde in phosphate-buffered saline (PBS) and stained as described previously (6). For immunohistochemistry, postnatal day 1.5 (P1.5) mice were transcardially perfused with a 4% paraformaldehyde PBS solution. Isolated brains were post-fixed with the paraformaldehyde solution for 3 h and submerged in PBS overnight. Tissues were then serially submerged in PBS containing 10% and 20% sucrose for 24 h and embedded in OCT compound. Frozen tissue was cut into 15-μm-thick sections using a cryostat. Nuclei were stained with Hoechst 33258 (Nacalai Tesque).

RESULTS

SOCS3-deficient NECs readily differentiate into astrocytes. RT-PCR analysis confirmed that SOCS3 mRNA was induced in NECs by LIF but not by BMP2 (data not shown). We

analyzed the properties of NECs lacking the *Socs3* gene in astrogliogenesis. The complete loss of the *Socs3* gene results in embryonic lethality due to a placental defect (30). Therefore, further analyses of the SOCS3 function in astrogliogenesis were done with NECs prepared from E14.5 *Socs3*-conditional knockout (*Socs3*-cKO) mice (18), in which Cre recombinase was expressed under the control of the nestin promoter to delete the loxP-flanked *Socs3* locus specifically in neural precursor cells. In normal mouse development, GFAP-positive astrocytes appear in the brain and spinal cord around the time of birth. For *Socs3*-cKO mice on P1.5, we found that GFAP immunoreactivity was significantly denser than that for normal littermates (Fig. 1A).

NECs from E14.5 wild-type and *Socs3*-cKO mice were cultured for 2 days in the absence or presence of LIF and stained for GFAP. No immunoreactivity to GFAP was observed in cultured NECs without LIF, regardless of the genotype (Fig. 1Ba and c). In the presence of LIF, GFAP immunoreactivity was obvious in SOCS3-deficient cells but not in wild-type cells (Fig. 1Bb and d). Considering the negative regulatory role of SOCS3, this result seemed reasonable at first glance, but in fact its interpretation was not as simple as was first thought: in 2-day cultures of wild-type NECs, GFAP-positive astrocytic differentiation has never been observed, even with a sufficiently high concentration of LIF, when BMP2 (or a BMP ligand) was not added (21). The result shown in Fig. 1Bd resembled the data obtained with the 2-day culture of NECs treated with LIF plus BMP2 (21). It was thus presumed that BMP signaling is unexpectedly activated in the LIF-stimulated, SOCS3-deficient NECs.

SOCS3 deficiency leads to unexpected Smad1 activation following LIF stimulation. In LIF-stimulated SOCS3-deficient NECs, we observed Smad1 activation, as detected by its serine phosphorylation, with a certain lag time compared to the expected sustained activation of STAT3, Erk1, and Erk2 (Fig. 2A). Immunocytochemistry confirmed that phosphorylated Smad1 had accumulated in the nuclei of LIF-treated SOCS3-deficient cells (Fig. 2B). Direct involvement of SOCS3 in the Smad signaling pathway was excluded, because wild-type and SOCS3-deficient cells exhibited comparable responses to BMP2 and BMP4 (see Fig. S1A in the supplemental material). In addition, overexpression of SOCS3 in NECs completely suppressed GFAP promoter activation by LIF, whereas SOCS3 did not have such a suppressive effect on BMP2-induced activation (see Fig. S1B in the supplemental material). When wild-type and SOCS3-deficient NECs were treated with BMP2, phosphorylation of Smad1 was detected within 30 min at a comparable level (see Fig. S1C in the supplemental material). Taken together, these findings implied that SOCS3 deficiency did not directly change the sensitivity of the cells to BMP2. Western blot analysis showed that in SOCS3-deficient NECs, phosphorylation of Smad1 began to be detected at around 3 h, peaked at around 6 h, and lasted until at least 12 h after LIF treatment (Fig. 2A and data not shown). Since the LIF-induced phosphorylation of Smad1 occurred much more slowly than that of STAT3, Erk1, and Erk2, it was suggested that LIF has a potential to activate (presumably in an indirect fashion) the Smad signaling pathway, which in normal cells is suppressed by SOCS3. A possibility is that LIF induces the production of BMP2 (and related BMP ligands, if any), which is under negative feedback regulation involving SOCS3.

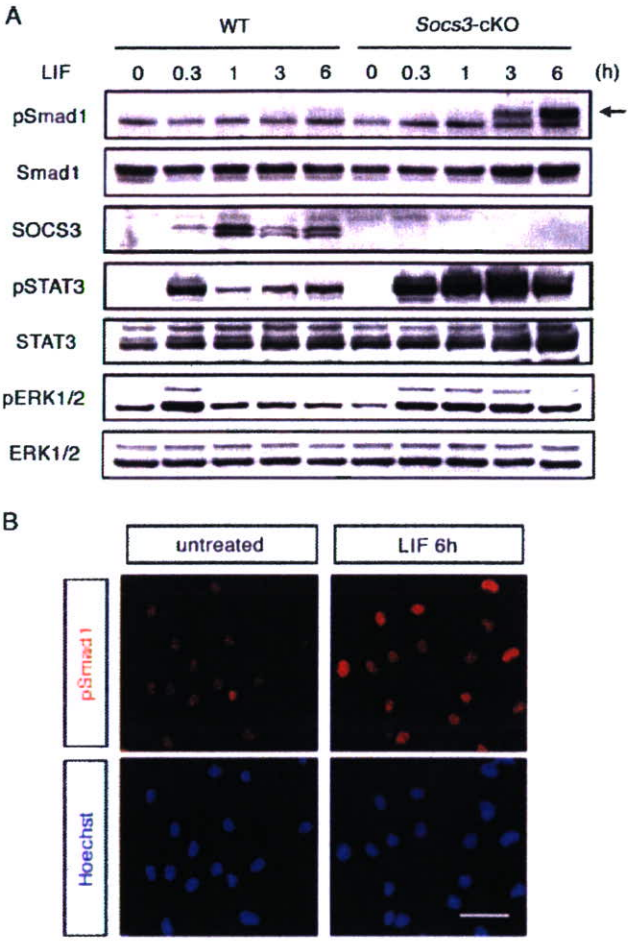

FIG. 2. SOCS3 deficiency leads to unexpected Smad1 activation following LIF stimulation. (A) Phosphorylation of STAT3, ERK1/2, and Smad1 in response to LIF. Wild-type and SOCS3-deficient cells were treated with LIF (50 ng/ml) for the indicated periods and solubilized. Cell lysates were separated by sodium dodecyl sulfate-polyacrylamide gel electrophoresis and subjected to Western blot analysis using the indicated antibodies by repeated reprobing. Arrow indicates the phosphorylated form of Smad1. (B) Nuclear localization of Smad1 after LIF treatment in SOCS3-deficient cells. Cells were either left untreated or exposed to LIF (50 ng/ml) and cultured for 6 h. The phosphorylated form of Smad1 and nuclei were detected by the anti-phospho-Smad1 antibody (red) and Hoechst 33258 staining (blue), respectively. Background levels of signals are shown in the upper left panel. Bar, 20 μm.

JAK-STAT signaling upregulates BMP2 production in NECs. We therefore assessed mRNAs for BMP2 in NECs upon LIF stimulation. As shown in Fig. 3A, BMP2 mRNA was upregulated at 3 h after LIF stimulation, and this upregulation was dramatically enhanced in the absence of SOCS3. Two identical potential STAT3 binding sites (5′-TTCAGAGAA-3′) were found in the 5′ flanking region of the mouse *Bmp2* gene (Fig. 3B). LIF treatment actually upregulated reporter expression downstream of the potential STAT3 binding sites, and overexpression of SOCS3 or a dominant-negative form of STAT3 (DN-STAT3) inhibited this LIF-induced reporter activation (Fig. 3C). Introduction of the mutation into this site (TTCAG AGAA→CCAAGAGAA) abrogated responsiveness to LIF

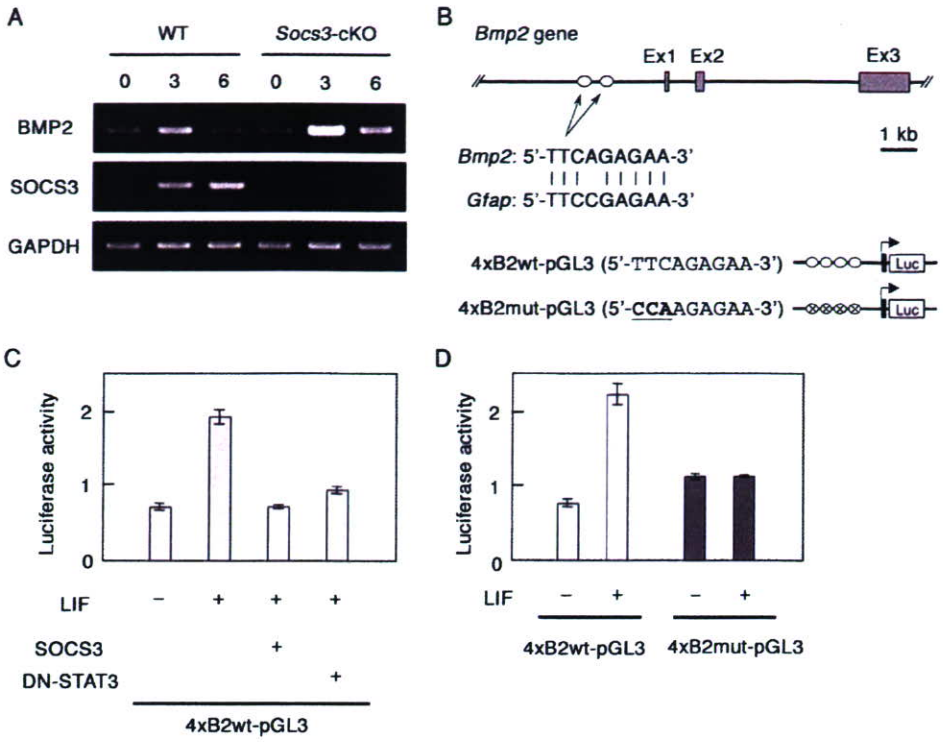

FIG. 3. LIF induces transcriptional activation of the *Bmp2* gene. (A) The induction of BMP2 transcripts in response to LIF was analyzed by RT-PCR. NECs were treated with LIF (50 ng/ml) for the indicated periods, and total RNAs were isolated. After the RT reaction, cDNA for BMP2 was amplified by PCR. cDNA for glyceraldehyde-3-phosphate dehydrogenase (GAPDH) was analyzed as a loading control. (B) Structures of the mouse *Bmp2* gene and reporter constructs used in this study. There are two identical potential STAT3 binding sites (5′-TTCAGAGAA-3′) in the 5′ region of the mouse *Bmp2* gene. Details about the reporter plasmids are given in Materials and Methods. (C) SOCS3-deficient MEFs were cotransfected with 4xB2wt-pGL3 and phRL-TK together with or without the expression plasmid of SOCS3 or DN-STAT3. Data are means ± standard deviations (error bars) derived from each assay performed in triplicate. (D) SOCS3-deficient MEFs were cotransfected with 4xB2wt-pGL3 or 4xB2mut-pGL3, together with phRL-TK. A luciferase assay was performed as for panel C.

(Fig. 4D). These results suggest the presence of a LIF-triggered positive pararegulatory loop involving STAT3-mediated induction of BMP2 expression and consequent activation of Smad1, which leads to efficient formation of an astrogliogenic nuclear complex containing STAT3, p300, and Smad1 (21).

To confirm this hypothesis, NECs were stimulated for 6 h by LIF in the presence of recombinant Noggin, which would block the effect of endogenously produced BMP2. As shown in Fig. 4A, LIF-induced phosphorylation of Smad1 in SOCS3-deficient cells was canceled by the addition of Noggin. When wild-type NECs were cultured for a much longer period (3 days) in the absence of LIF, a phosphorylated form of Smad1 was weakly detected (Fig. 4B), possibly due to endogenously produced and accumulated BMP ligands. Importantly, the amount of phosphorylated Smad1 was significantly enhanced by the addition of LIF, which was inhibited by Noggin (Fig. 4B).

We previously reported that, in 4-day NEC cultures, LIF alone or BMP2 alone could induce differentiation of GFAP-positive astrocytes, while medium alone had no such effect (6, 22, 38). Our interpretation was that this was due to accumulation of BMP ligands that had been produced spontaneously by NECs during the 4-day culture and that cooperate with exogenously added LIF (22). Actually, RT-PCR analysis showed that NECs express LIF and BMP2, though at relatively low levels, and GFAP-positive astrocytic differentiation was observed in a 16-day culture of NECs without exogenously added LIF or BMP2 (22). As shown in Fig. 4C, Noggin suppressed the differentiation of GFAP-positive astrocytes from wild-type NECs in the 4-day LIF-containing culture. Our current results provide a revised interpretation for astrocytic differentiation of NECs by LIF alone in the 4-day cultures: LIF upregulated the expression of BMP2 and cooperated with the accumulated BMP protein to induce astrocytes. SOCS3-deficient NECs after 4-day culture with LIF displayed more-intense GFAP immunoreactivity than wild-type cells, and this immunoreactivity was reduced by Noggin (Fig. 4D). Notably, the GFAP-expressing cells of these two different genotypes represented morphologically distinct cell types: wild-type cells showed an elongated bipolar morphology in most cases (Fig. 4C, left panel), while, in marked contrast, SOCS3-deficient cells displayed a widespread and highly branched stellate morphology (Fig. 4D, left panel). This morphological observation could not simply be explained by the enhanced LIF-STAT3 signaling due to SOCS3 deficiency; it reminded us of a recent report showing that BMP4 treatment of neural progenitors leads to the appearance of GFAP-expressing cells with a widespread stellate morphology having an increased number of processes, whereas LIF treatment induces a bipolar or tripolar morphology (1).

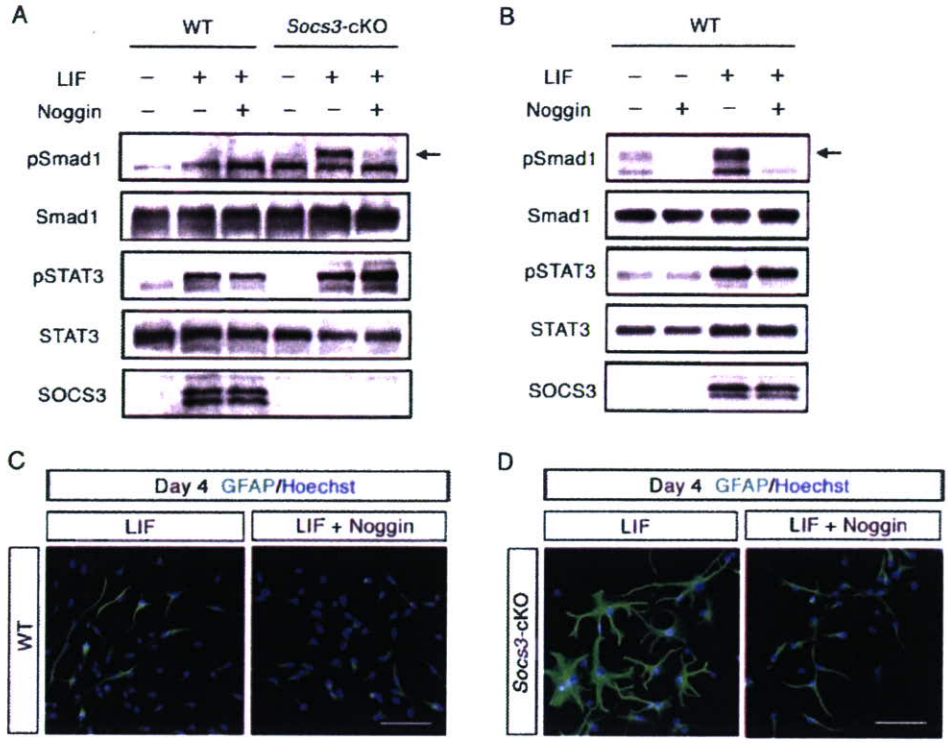

FIG. 4. LIF induces Smad1 activation through the expression of BMP2. (A) Effect of Noggin on LIF-induced phosphorylation of Smad1. Wild-type and SOCS3-deficient cells were treated with LIF (50 ng/ml) together with or without Noggin (200 ng/ml). Cell lysates were prepared after 6 h of incubation. Western blot analysis was performed as for Fig. 2A. Arrow indicates the phosphorylated form of Smad1. (B) Phosphorylation of Smad1 by LIF after the 3-day culture. A total of 2×10^5 wild-type cells were plated on 3.5-cm-diameter dishes and treated with LIF (80 ng/ml) together with or without Noggin (200 ng/ml). (C) Noggin suppressed the LIF-induced differentiation of GFAP-positive astrocytes from wild-type NECs. NECs derived from wild-type mice were cultured with LIF (80 ng/ml) in the absence (left) or in the presence (right) of Noggin (200 ng/ml). Cells were fixed and stained with an anti-GFAP antibody (green). Nuclei were stained with Hoechst 33258 (blue). Bar, 50 μm. (D) Effects of Noggin on the morphological changes of SOCS3-deficient NECs after the 4-day culture with LIF. Noggin treatment and immunostaining were performed as for panel C.

DISCUSSION

Our present study revealed a positive pararegulatory loop involving STAT3-mediated induction of BMP2 expression and subsequent Smad1 activation (Fig. 5). This newly found loop appears to function as a signal booster for astrogliogenesis triggered by IL-6 family cytokines, in the sense that STAT3 induces Smad1 activation to form the astrogliogenic STAT3-p300-Smad complex. Noggin treatment, which blocked the pararegulatory loop and abrogated astrogliogenic differentiation (Fig. 4C), indicated that this signal booster mechanism is crucial for astrogliogenesis. In addition to this loop, a recent study proposed the presence of a positive autoregulatory loop of JAK-STAT signaling that involves STAT3-mediated upregulated expression of STAT1, STAT3, and gp130 (9) (Fig. 5). Both of these positive loops triggered by IL-6 family cytokines are under the negative feedback regulation of SOCS3 (Fig. 5).

Although LIF and BMP2 cooperate in that they synergistically induce GFAP-positive astrocytes, they affect astrocyte morphology differently (1). The morphological difference in BMP-treated and LIF-treated neural progenitors has also been reported previously (22, 29). LIF-stimulated SOCS3-deficient cells in our current study (Fig. 4D) displayed a morphology similar to that observed for cells under BMP stimulation (1). A notable change in morphology was observed in the Noggin-containing culture; LIF-stimulated SOCS3-deficient NECs exhibited a bipolar or tripolar shape (Fig. 4D, right panel) compared to the widespread and well-branched shape without Noggin (Fig. 4D, left panel). Our present study indicated that the BMP-Smad pathway was activated, in addition to the LIF-STAT3 pathway, in astrogliogenesis. Mechanisms for such morphological changes may involve cytokine-inducible cytoskeletal rearrangements, such as BMP-induced activation of LIM kinase 1, a key regulator of actin dynamics (5).

LIF has been reported to promote astrogliogenesis and, paradoxically, to support neural stem cell renewal as well (11, 13, 27). Further molecular characterization of the pararegulatory loop clarified in this study may explain the differential effect of LIF on neural precursor cells. In nonneural cell systems, it has recently been shown that STAT3 upregulates transforming growth factor β1 expression in hepatocytes and T cells, which is downregulated by SOCS3 (12, 24). Two other groups have shown a negative effect of STAT1 and STAT3 on Smad signaling through the transcriptional upregulation of Smad7 (10, 40). In this sense, JAK-STAT signaling is supposed to have two distinct roles as a modulator of transforming

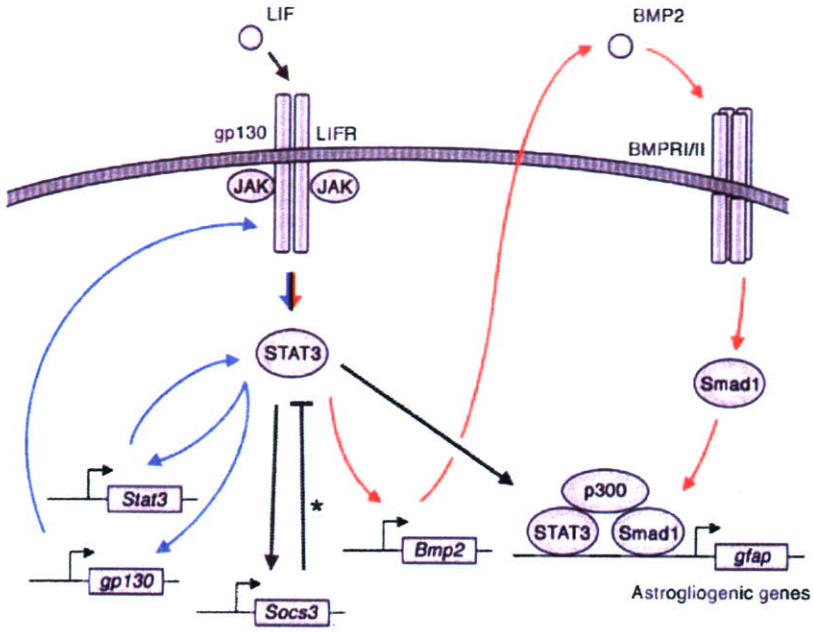

FIG. 5. Model of LIF-triggered activation of JAK-STAT and Smad signaling pathways in astrogliogenesis. Red arrows indicate the positive pararegulatory loop shown in this study. Asterisk indicates negative feedback. Blue arrows indicate the previously reported positive autoregulatory loop of JAK-STAT signaling (9).

growth factor β superfamily signaling pathways, depending on the cellular context.

Proteins of the SOCS family show broad spatial patterns of expression in the developing and adult mouse CNS (28). Emery et al. in 2006 reported properties of SOCS3-deficient neural precursor cells derived from E10.5 embryos by mating *Socs3* heterozygous mutant mice (4). In their report, Northern blot analysis indicated that LIF-induced GFAP mRNA expression was potentiated in SOCS3-deficient cells, consistent with our present observation. However, SOCS3-deficient cells cultured in the presence of LIF grew as small aggregates (Fig. 6 in reference 4) rather than displaying the widespread and highly branched stellate morphology shown in our study (Fig. 4D). The reason for this discrepancy is not known at the moment, but different culture conditions and cell preparation procedures may have influenced the expression of LIF-downstream genes besides GFAP. It is of interest whether AMOG, which was identified as a LIF response gene in our microarray study, regulates cell-cell and cell-substrate interactions in NECs as in human glioma cells (32). In contrast to SOCS3 (3), SOCS2 had no inhibitory effect on LIF-induced astrocytic differentiation (see Fig. S2 in the supplemental material). Considering the previously reported role of SOCS2 in the neuronal cell lineage (39), SOCS3 and SOCS2 appear to have different roles in the brain depending on cell types and upstream cytokines.

In addition to the developing brain, SOCS3-upstream cytokines function in tissues and organs under inflammatory conditions. Injury in the adult spinal cord results in rapid expression of IL-6 family cytokines (35), followed by the induction of SOCS3 (23). Okada et al. recently observed escalated accumulation of reactive astrocytes in the injured spinal cords of *Socs3*-cKO mice compared to wild-type mice (25). It is possible that SOCS3 prevents the development and/or accumulation of reactive astrocytes at the injured site by inhibiting both the autoregulatory and the pararegulatory loop (see Fig. 5). Upregulation of BMP2 and BMP7 mRNAs was observed after spinal cord injury (33, 34); the kinetics of this upregulation were slow and biphasic (34), which may be attributed, in part, to the IL-6 family cytokine-induced pararegulatory positive loop involving BMP production found in the present study. Further investigations to elucidate the orchestration of the cytokine network would provide valuable clues not only for fuller understanding of the regulation of neural stem cells but also for the development of a therapeutic target for cytokine-induced nerve degeneration and regeneration.

ACKNOWLEDGMENTS

We thank H. Okano (Keio University) and S. Noguchi (Meiji Milk Products) for Nestin-Cre transgenic mice, T. Kitamura (University of Tokyo) for the retroviral system, and Astellas Pharma Inc. for BMP2. We also thank I. Nobuhisa for valuable discussions; M. Teramoto, N. Oga, and C. Okamura for secretarial assistance; and Y. Saiki, K. Fujimoto, S. Iwaki, and S. Usuki for technical help.

This work was supported by 21st Century COE grant "Cell Fate Regulation Research and Education Unit," Grant-in-Aid for Scientific Research (B), and by Grant-in-Aid for Scientific Research on Priority Areas "Molecular Brain Science" and "Self-Renewal and Pluripotency of Stem Cells" from MEXT Japan. This work was also supported in part by CREST, JST.

REFERENCES

1. **Bonaguidi, M. A., T. McGuire, M. Hu, L. Kan, J. Samanta, and J. A. Kessler.** 2005. LIF and BMP signaling generate separate and discrete types of GFAP-expressing cells. Development **132**:5503–5514.
2. **Bonni, A., Y. Sun, M. Nadal-Vicens, A. Bhatt, D. A. Frank, I. Rozovsky, N. Stahl, G. D. Yancopoulos, and M. E. Greenberg.** 1997. Regulation of gliogenesis in the central nervous system by the JAK-STAT signaling pathway. Science **278**:477–483.
3. **Cao, F., R. Hata, P. Zhu, Y. J. Ma, J. Tanaka, Y. Hanakawa, K. Hashimoto, M. Niinobe, K. Yoshikawa, and M. Sakanaka.** 2006. Overexpression of

SOCS3 inhibits astrogliogenesis and promotes maintenance of neural stem cells. J. Neurochem. **98**:459–470.
4. **Emery, B., T. D. Merson, C. Snell, K. M. Young, M. Ernst, and T. J. Kilpatrick.** 2006. SOCS3 negatively regulates LIF signaling in neural precursor cells. Mol. Cell. Neurosci. **31**:739–747.
5. **Foletta, V. C., M. A. Lim, J. Soosairajah, A. P. Kelly, E. G. Stanley, M. Shannon, W. He, S. Das, J. Massague, and O. Bernard.** 2003. Direct signaling by the BMP type II receptor via the cytoskeletal regulator LIMK1. J. Cell Biol. **162**:1089–1098.
6. **Fukuda, S., T. Kondo, H. Takebayashi, and T. Taga.** 2004. Negative regulatory effect of an oligodendrocytic bHLH factor OLIG2 on the astrocytic differentiation pathway. Cell Death Differ. **11**:196–202.
7. **Jessen, K. R., and W. D. Richardson.** 2001. Glial cell development: basic principles and clinical relevance, 2nd ed. Oxford University Press, New York, NY.
8. **Gross, R. E., M. F. Mehler, P. C. Mabie, Z. Zang, L. Santschi, and J. A. Kessler.** 1996. Bone morphogenetic proteins promote astroglial lineage commitment by mammalian subventricular zone progenitor cells. Neuron **17**: 595–606.
9. **He, F., W. Ge, K. Martinowich, S. Becker-Catania, V. Coskun, W. Zhu, H. Wu, D. Castro, F. Guillemot, G. Fan, J. de Vellis, and Y. E. Sun.** 2005. A positive autoregulatory loop of Jak-STAT signaling controls the onset of astrogliogenesis. Nat. Neurosci. **8**:616–625.
10. **Jenkins, B. J., D. Grail, T. Nheu, M. Najdovska, B. Wang, P. Waring, M. Inglese, R. M. McLoughlin, S. A. Jones, N. Topley, H. Baumann, L. M. Judd, A. S. Giraud, A. Boussioutas, H. J. Zhu, and M. Ernst.** 2005. Hyperactivation of Stat3 in gp130 mutant mice promotes gastric hyperproliferation and desensitizes TGF-β signaling. Nat. Med. **11**:845–852.
11. **Kamakura, S., K. Oishi, T. Yoshimatsu, M. Nakafuku, N. Masuyama, and Y. Gotoh.** 2004. Hes binding to STAT3 mediates crosstalk between Notch and JAK-STAT signalling. Nat. Cell Biol. **6**:547–554.
12. **Kinjyo, I., H. Inoue, S. Hamano, S. Fukuyama, T. Yoshimura, K. Koga, H. Takaki, K. Himeno, G. Takaesu, T. Kobayashi, and A. Yoshimura.** 2006. Loss of SOCS3 in T helper cells resulted in reduced immune responses and hyperproduction of interleukin 10 and transforming growth factor-β1. J. Exp. Med. **203**:1021–1031.
13. **Koblar, S. A., A. M. Turnley, B. J. Classon, K. L. Reid, C. B. Ware, S. S. Cheema, M. Murphy, and P. F. Bartlett.** 1998. Neural precursor differentiation into astrocytes requires signaling through the leukemia inhibitory factor receptor. Proc. Natl. Acad. Sci. USA **95**:3178–3181.
14. **Kubo, M., T. Hanada, and A. Yoshimura.** 2003. Suppressors of cytokine signaling and immunity. Nat. Immunol. **4**:1169–1176.
15. **Liu, Y., S. S. Han, Y. Wu, T. M. Tuohy, H. Xue, J. Cai, S. A. Back, L. S. Sherman, I. Fischer, and M. S. Rao.** 2004. CD44 expression identifies astrocyte-restricted precursor cells. Dev. Biol. **276**:31–46.
16. **Lu, Y., S. Fukuyama, R. Yoshida, T. Kobayashi, K. Saeki, H. Shiraishi, A. Yoshimura, and G. Takaesu.** 2006. Loss of SOCS3 gene expression converts STAT3 function from anti-apoptotic to pro-apoptotic. J. Biol. Chem. **281**: 36683–36690.
17. **Massague, J., and D. Wotton.** 2000. Transcriptional control by the TGF-β/Smad signaling system. EMBO J. **19**:1745–1754.
18. **Mori, H., R. Hanada, T. Hanada, D. Aki, R. Mashima, H. Nishinakamura, T. Torisu, K. R. Chien, H. Yasukawa, and A. Yoshimura.** 2004. Socs3 deficiency in the brain elevates leptin sensitivity and confers resistance to diet-induced obesity. Nat. Med. **10**:739–743.
19. **Nakashima, K., T. Takizawa, W. Ochiai, M. Yanagisawa, T. Hisatsune, M. Nakafuku, K. Miyazono, T. Kishimoto, R. Kageyama, and T. Taga.** 2001. BMP2-mediated alteration in the developmental pathway of fetal mouse brain cells from neurogenesis to astrocytogenesis. Proc. Natl. Acad. Sci. USA **98**:5868–5873.
20. **Nakashima, K., S. Wiese, M. Yanagisawa, H. Arakawa, N. Kimura, T. Hisatsune, K. Yoshida, T. Kishimoto, M. Sendtner, and T. Taga.** 1999. Developmental requirement of gp130 signaling in neuronal survival and astrocyte differentiation. J. Neurosci. **19**:5429–5434.
21. **Nakashima, K., M. Yanagisawa, H. Arakawa, N. Kimura, T. Hisatsune, M. Kawabata, K. Miyazono, and T. Taga.** 1999. Synergistic signaling in fetal brain by STAT3-Smad1 complex bridged by p300. Science **284**:479–482.
22. **Nakashima, K., M. Yanagisawa, H. Arakawa, and T. Taga.** 1999. Astrocyte differentiation mediated by LIF in cooperation with BMP2. FEBS Lett. **457**:43–46.
23. **Nesic, O., N. M. Svrakic, G. Y. Xu, D. McAdoo, K. N. Westlund, C. E. Hulsebosch, Z. Ye, A. Galante, P. Soteropoulos, P. Tolias, W. Young, R. P. Hart, and J. R. Perez-Polo.** 2002. DNA microarray analysis of the contused spinal cord: effect of NMDA receptor inhibition. J. Neurosci. Res. **68**:406–423.
24. **Ogata, H., T. Chinen, T. Yoshida, I. Kinjyo, G. Takaesu, H. Shiraishi, M. Iida, T. Kobayashi, and A. Yoshimura.** 2006. Loss of SOCS3 in the liver promotes fibrosis by enhancing STAT3-mediated TGF-β1 production. Oncogene **25**:2520–2530.
25. **Okada, S., M. Nakamura, H. Katoh, T. Miyao, T. Shimazaki, K. Ishii, J. Yamane, A. Yoshimura, Y. Iwamoto, Y. Toyama, and H. Okano.** 2006. Conditional ablation of Stat3 or Socs3 discloses a dual role for reactive astrocytes after spinal cord injury. Nat. Med. **12**:829–834.
26. **Pagliusi, S. R., M. Schachner, P. H. Seeburg, and B. D. Shivers.** 1990. The adhesion molecule on glia (AMOG) is widely expressed by astrocytes in developing and adult mouse brain. Eur. J. Neurosci. **2**:471–480.
27. **Pitman, M., B. Emery, M. Binder, S. Wang, H. Butzkueven, and T. J. Kilpatrick.** 2004. LIF receptor signaling modulates neural stem cell renewal. Mol. Cell. Neurosci. **27**:255–266.
28. **Polizzotto, M. N., P. F. Bartlett, and A. M. Turnley.** 2000. Expression of "suppressor of cytokine signalling" (SOCS) genes in the developing and adult mouse nervous system. J. Comp. Neurol. **423**:348–358.
29. **Rajan, P., D. M. Panchision, L. F. Newell, and R. D. McKay.** 2003. BMPs signal alternately through a SMAD or FRAP-STAT pathway to regulate fate choice in CNS stem cells. J. Cell Biol. **161**:911–921.
30. **Roberts, A. W., L. Robb, S. Rakar, L. Hartley, L. Cluse, N. A. Nicola, D. Metcalf, D. J. Hilton, and W. S. Alexander.** 2001. Placental defects and embryonic lethality in mice lacking suppressor of cytokine signaling 3. Proc. Natl. Acad. Sci. USA **98**:9324–9329.
31. **Sauvageot, C. M., and C. D. Stiles.** 2002. Molecular mechanisms controlling cortical gliogenesis. Curr. Opin. Neurobiol. **12**:244–249.
32. **Scheidenhelm, D. K., J. Cresswell, C. A. Haipek, T. P. Fleming, R. W. Mercer, and D. H. Gutmann.** 2005. Akt-dependent cell size regulation by the adhesion molecule on glia occurs independently of phosphatidylinositol 3-kinase and Rheb signaling. Mol. Cell. Biol. **25**:3151–3162.
33. **Setoguchi, T., K. Nakashima, T. Takizawa, M. Yanagisawa, W. Ochiai, M. Okabe, K. Yone, S. Komiya, and T. Taga.** 2004. Treatment of spinal cord injury by transplantation of fetal neural precursor cells engineered to express BMP inhibitor. Exp. Neurol. **189**:33–44.
34. **Setoguchi, T., K. Yone, E. Matsuoka, H. Takenouchi, K. Nakashima, T. Sakou, S. Komiya, and S. Izumo.** 2001. Traumatic injury-induced BMP7 expression in the adult rat spinal cord. Brain Res. **921**:219–225.
35. **Streit, W. J., S. L. Semple-Rowland, S. D. Hurley, R. C. Miller, P. G. Popovich, and B. T. Stokes.** 1998. Cytokine mRNA profiles in contused spinal cord and axotomized facial nucleus suggest a beneficial role for inflammation and gliosis. Exp. Neurol. **152**:74–87.
36. **Taga, T., and T. Kishimoto.** 1997. gp130 and the interleukin-6 family of cytokines. Annu. Rev. Immunol. **15**:797–819.
37. **Takeda, T., K. Nakajima, H. Kojima, and T. Hirano.** 1994. E1A repression of IL-6-induced gene activation by blocking the assembly of IL-6 response element binding complexes. J. Immunol. **153**:4573–4582.
38. **Takizawa, T., K. Nakashima, M. Namihira, W. Ochiai, A. Uemura, M. Yanagisawa, N. Fujita, M. Nakao, and T. Taga.** 2001. DNA methylation is a critical cell-intrinsic determinant of astrocyte differentiation in the fetal brain. Dev. Cell **1**:749–758.
39. **Turnley, A. M., C. H. Faux, R. L. Rietze, J. R. Coonan, and P. F. Bartlett.** 2002. Suppressor of cytokine signaling 2 regulates neuronal differentiation by inhibiting growth hormone signaling. Nat. Neurosci. **5**:1155–1162.
40. **Ulloa, L., J. Doody, and J. Massague.** 1999. Inhibition of transforming growth factor-beta/SMAD signalling by the interferon-gamma/STAT pathway. Nature **397**:710–713.
41. **Wright, L. S., J. Li, M. A. Caldwell, K. Wallace, J. A. Johnson, and C. N. Svendsen.** 2003. Gene expression in human neural stem cells: effects of leukemia inhibitory factor. J. Neurochem. **86**:179–195.

Development/Plasticity/Repair

Epigenetic Modulation of Seizure-Induced Neurogenesis and Cognitive Decline

Sebastian Jessberger,[1] Kinichi Nakashima,[4] Gregory D. Clemenson Jr,[1] Eunice Mejia,[1] Emily Mathews,[1] Kerstin Ure,[2] Shiori Ogawa,[3] Christopher M. Sinton,[3] Fred H. Gage,[1] and Jenny Hsieh[2]

[1]Laboratory of Genetics, Salk Institute for Biological Studies, La Jolla, California 92037, [2]Department of Molecular Biology, Cecil H. and Ida Green Center for Reproductive Biology Sciences and [3]Department of Internal Medicine, University of Texas Southwestern Medical Center, Dallas, Texas 75390, and [4]Laboratory of Molecular Neuroscience, Nara Institute of Science and Technology, Ikoma 630-0101, Japan

The conceptual understanding of hippocampal function has been challenged recently by the finding that new granule cells are born throughout life in the mammalian dentate gyrus (DG). The number of newborn neurons is dynamically regulated by a variety of factors. Kainic acid-induced seizures, a rodent model of human temporal lobe epilepsy, strongly induce the proliferation of DG neurogenic progenitor cells and are also associated with long-term cognitive impairment. We show here that the antiepileptic drug valproic acid (VPA) potently blocked seizure-induced neurogenesis, an effect that appeared to be mainly mediated by inhibiting histone deacetylases (HDAC) and normalizing HDAC-dependent gene expression within the epileptic dentate area. Strikingly, the inhibition of aberrant neurogenesis protected the animals from seizure-induced cognitive impairment in a hippocampus-dependent learning task. We propose that seizure-generated granule cells have the potential to interfere with hippocampal function and contribute to cognitive impairment caused by epileptic activity within the hippocampal circuitry. Furthermore, our data indicate that the effectiveness of VPA as an antiepileptic drug may be partially explained by the HDAC-dependent inhibition of aberrant neurogenesis induced by seizure activity within the adult hippocampus.

Key words: valproic acid; neurogenesis; hippocampus; seizure; object recognition; learning; histone deacetylase

Introduction

The hippocampal subgranular zone contains cells that continue to divide and differentiate into neurons throughout adulthood (Gage, 2000). Adult neurogenesis can be enhanced by a number of extrinsic factors, including exercise, enriched environment, and learning (Kempermann et al., 1997; Gould et al., 1999; Van Praag et al., 1999). Experimental insults, such as status epilepticus (SE), can also cause a marked increase in adult neurogenesis (Bengzon et al., 1997; Parent et al., 1997; Scott et al., 1998). It has been speculated that seizure-induced neurogenesis contributes to the deficits in hippocampal learning and memory that are associated with SE (Stafstrom et al., 1993; Holmes, 1997; Parent, 2002; Parent and Lowenstein, 2002).

Valproic acid (VPA) (2-propylpentanoic acid) is a well known anticonvulsant and mood stabilizer (Henry, 2003). Recently, VPA has been shown to directly inhibit histone deacetylases (HDACs) (Gottlicher et al., 2001; Phiel et al., 2001). HDACs belong to a family of enzymes that modify the N-terminal tails of histones, altering the interaction between histones and DNA and serving as an epigenetic regulator of gene expression. Huang et al. (2002) reported that changes in glutamate receptor 2 (GluR2) and brain-derived neurotrophic factor (BDNF) after pilocarpine-induced SE were associated with increased histone acetylation in a promoter-specific manner. Both GluR2 and BDNF contain a neuron-restrictive silencing element (*NRSE*), which is a consensus 21 bp DNA binding site for the neuron-restrictive silencing factor [NRSF, also called repressor element 1 (RE1)-silencing transcription factor (REST)] (Chong et al., 1995; Schoenherr and Anderson, 1995). NRSF transcripts are rapidly induced in the hippocampus after seizures (Palm et al., 1998). Recent work from our laboratory has shown that NRSF also functions as an activator of gene expression in adult neural stem cells to induce neurogenesis (Kuwabara et al., 2004). In undifferentiated neural progenitors or in glial cells, NRSF can associate with repressor proteins such as HDACs and/or methyl-DNA binding proteins (such as methyl-CpG binding protein 2) to repress neuronal gene expression (Naruse et al., 1999; Ballas et al., 2001). However, in neuroblasts, NRSF interacts with a noncoding RNA with the same sequence as the *NRSE* to activate gene expression and promote neuronal differentiation (Kuwabara et al., 2004). We previously reported that VPA blocked the proliferation and

Received Jan. 10, 2007; revised April 23, 2007; accepted April 26, 2007.

S.J. was supported in part by the Deutsche Forschungsgemeinschaft (Je297/1-1) and the American Epilepsy Society. J.H. was supported in part by The Esther A. and Joseph Klingenstein Fund, The Ellison Medical Foundation, and The Advanced Research Program, Texas Higher Education Coordinating Board. Additional support was provided by grants from the National Institute of Neurological Disorders and Stroke/National Institute on Aging, the Max Planck Research Award Program funded by the German Ministry for Education, Science, Research, and Technology, and the Pritzker Research Consortium (F.H.G.). We thank members of the Gage laboratory for helpful discussions and M. L. Gage for editorial comments. We also thank Nicola J. Broadbent and Robert E. Clark (University of California, San Diego, La Jolla, CA) for help with the object recognition testing.

Correspondence should be addressed to either of the following: Fred H. Gage, Laboratory of Genetics, Salk Institute for Biological Studies, La Jolla, CA 92037, E-mail: gage@salk.edu; or Jenny Hsieh, Department of Molecular Biology, Cecil H. and Ida Green Center for Reproductive Biology Sciences, University of Texas Southwestern Medical Center, Dallas, TX 75390, E-mail: jenny.hsieh@utsouthwestern.edu.

DOI:10.1523/JNEUROSCI.0110-07.2007

 0270-6474/07/275967-09$15.00/0

induced neuronal differentiation of adult hippocampal neural progenitor cells *in vitro* and *in vivo* (Hsieh et al., 2004). This effect of VPA was associated with a hyperacetylation of histones and an upregulation of NRSF-regulated neuronal genes (Hsieh et al., 2004).

Here we examined the effects of the HDAC inhibitor VPA on kainic acid (KA)-induced seizures. We found that VPA inhibited seizure-induced neurogenesis and reduced abnormal morphological changes of newborn neurons to the level seen in control animals. The ability of VPA to inhibit seizure-induced neurogenesis was associated with increase in NRSF mRNA as well as altered expression levels of several NRSF-regulated neuronal genes. VPA treatment potently protected epileptic animals from hippocampus-dependent cognitive impairment after KA-induced seizures. The data presented support the notion that increased neurogenesis after SE is essentially aberrant and might contribute to pathological changes associated with epileptic activity within the hippocampal circuitry.

Materials and Methods

Animals. Sixty adult female Fisher 344 rats (180–200 g) were used in this study. To induce SE, rats were injected with KA (12 mg/kg, i.p.). Seizure activity was monitored behaviorally, and only animals exhibiting 3 h of continuous convulsive SE were included in these experiments. Five hours after the onset of seizures, rats in the VPA groups received their first VPA injection (150 mg/kg twice daily, i.p.) that has been shown previously to inhibit HDACs *in vivo* (Shen et al., 2005; Winkler et al., 2005). Control animals received injections of identical volumes of saline. The day after seizure induction, all rats received daily injections of bromodeoxyuridine (BrdU) (50 mg/kg, i.p.) for 7 d. Rats in the proliferation group were killed 1 d after the last BrdU injection (controls, $n = 8$; KA, $n = 11$). Rats in the survival group survived for 4 more weeks (controls, $n = 8$; KA, $n = 10$). VPA was injected twice daily throughout the entire length of the experiment (7 d in the proliferation group and 5 weeks in the survival group).

In a separate experiment, six adult female Fisher 344 rats (180–200 g) were chronically implanted with electroencephalographic/electromyographic (EEG/EMG) electrodes and allowed to recover from surgery for 3 weeks (see below). After habituation, rats were injected with KA, and, 5 h after the onset of SE, animals were injected with either VPA (300 mg/kg, i.p.) ($n = 3$) or saline vehicle controls ($n = 3$) and we began EEG/EMG monitoring, which continued for 3 d. During the following 2 d, VPA (300 mg/kg, i.p.) or saline was injected once a day.

To obtain hippocampal RNA for reverse transcription (RT)-PCR (see below), eight adult female Fisher rats (180–200 g) were injected with KA alone or with KA after a "preinjection" with VPA (300 mg/kg, i.p.) or trichostatin A (TSA) (1 mg/kg, i.p.) 1 h before the induction of SE. Rats were killed 3 or 24 h after the onset of seizures. In a subsequent experiment, VPA, TSA, or valpromide (100 mg/kg, i.p.) was given 5 h after KA-induced seizure onset (plus saline and KA only controls), and the hippocampi were harvested 24 h later. An additional six rats was used for the KA time course RT-PCR (see Fig. 4*A*) and eight rats for the KA time course Western blots (see Fig. 4*B*).

Preparation of hippocampal tissue, RT-PCR, and Western blots. The hippocampus of both hemispheres was dissected out and chopped into 1-mm-thick coronal slices (McIlwain tissue chopper). The dentate gyrus (DG), CA3, and CA1 were carefully isolated using a dissection microscope. RNA isolation from the obtained tissue and cDNA synthesis were performed as described previously (Hsieh et al., 2004). Primer sequences are available on request. Glyceraldehyde-3-phosphate dehydrogenase (GAPDH) and β-actin were used as normalization controls. Western blot analysis was performed essentially as described previously with slight modifications (Hsieh et al., 2004). Protein lysates from the obtained tissue were solubilized in standard radioimmunoprecipitation assay buffer and homogenized by doing three pulses for 10 s each on ice at setting 1 (Tissue Tearor; Biospec, Bartlesville, OK). Supernatants were normalized for total protein concentration using a BCA protein assay kit (Pierce, Rockford, IL) and separated by SDS-PAGE (NuPage 7% Tris–acetate gel; Invitrogen, Carlsbad, CA). Primary antibodies were rabbit anti-REST (1:500; Upstate Biotechnology, Lake Placid, NY), rabbit anti-GluR2/3 (1:500; Millipore, Temecula, CA), and mouse anti-GAPDH (1:2500; Millipore). Secondary antibodies were anti-rabbit (1:750) or anti-mouse (1:1000) horseradish peroxidase from Cell Signaling Technology (Beverly, MA), and chemiluminescence signals were detected with ECL plus detection kit (GE Healthcare, Little Chalfont, UK) and exposed to film.

Immunohistochemistry. Animals were anesthetized with a ketamine/xylazine mixture and perfused with 0.9% NaCl solution, followed by 4% paraformaldehyde (PFA) in 0.1 M phosphate buffer, pH 7.4. Brains were postfixed in 4% PFA for 24 h and then transferred into 30% sucrose. Forty micrometer coronal section series were cut using a sliding microtome. All staining was done with free-floating sections. For BrdU detection, the sections were pretreated with 2N HCl for 30 min at 37°C and washed in 0.1 M borate buffer, pH 8.5, for 10 min.

To determine the absolute number of BrdU-labeled cells and to visualize the morphology of doublecortin (DCX)-positive cells, the peroxidase method (ABC system; Vectastain; Vector Laboratories, Burlingame, CA) with biotinylated anti-rat and anti-goat antibodies and nickel-intensified diaminobenzidine (Sigma, St. Louis, MO) as chromogen was used. Immunofluorescent triple labeling was done as described previously (Jessberger and Kempermann, 2003). As primary antibodies, we used rat anti-BrdU (1:500; Harlan Sera-Lab, Loughborough, UK), mouse anti-neuronal neuclei (NeuN) (1:100; Millipore), goat anti-doublecortin (1:250; Santa Cruz Biotechnology, Santa Cruz, CA), rabbit anti-S100β (1:1000; Swant, Bellinzona, Switzerland), rabbit anti-Ki67 (1:250; Novocastra Laboratories, Newcastle upon Tyne, UK), and rabbit-anti-REST (1:100; Upstate Biotechnology). To determine the extension of basal dendrites arising from new neurons, we captured 12 images of the granule cell layer (GCL) spanning 250 μm in length for each animal. Images were exported into Adobe Photoshop 7.0 (Adobe Systems, San Jose, CA), and three zones starting from the inner border of the GCL and stretching 20 μm apart from each other were outlined. All processes in each zone were counted.

For Fluoro-Jade B staining, sections were mounted on coated slides and dried for 24 h at room temperature. The sections were rehydrated, washed for 2 min in ddH_2O, blocked in 0.06% potassium permanganate, and incubated for 30 min in the staining solution with 0.0008% Fluoro-Jade B (Millipore).

Cell counts. The total number of BrdU-positive cells was counted using every 12th section (480 μm apart) from all animals. BrdU-positive cells were counted throughout the rostrocaudal extent of the granule cell layer using a 20× objective and a conventional bright-field microscope (Eclipse E800; Nikon, Tokyo, Japan) as described previously (Kempermann and Gage, 1999). Derived numbers were multiplied by 12 to obtain total cell numbers per GCL.

One-in-12 series of sections from animals from the proliferation group and the survival group (see Fig. 1) were double stained for Ki67/DCX or BrdU and NeuN. Fluorescent signals were detected using a spectral confocal microscope (Radiance 2100; Bio-Rad, Hercules, CA). All analyses were performed in sequential scanning mode, and double labeling was confirmed by three-dimensional reconstructions of *z*-series. From each animal, 50 Ki67-positive (proliferation group) or BrdU-positive (survival group) cells were randomly picked throughout the GCL and analyzed. Images were processed with Adobe Photoshop 7.0, and only general contrast enhancements and color level adjustments were performed.

Stereological counting of the hippocampal subfields was done as described previously (Kempermann et al., 1997). StereoInvestigator software (MicroBrightField, Williston, VT) controlling an epifluorescence microscope (Nikon Eclipse E600) was used. The grid size for the granule cell layer was 150 μm^2 and for the CA fields was 250 μm^2. The counting frame size for the GCL was 10 μm^2 and for the CA fields was 15 μm^2. The coefficient of error (Gundersen) was between 0.07 and 0.15 for the GCL and 0.08 and 0.31 for the CA fields.

Behavioral analysis. All animals in the survival groups were tested in a hippocampus-dependent object recognition task (controls, $n = 8$; KA, $n = 10$). Rats were habituated to the testing room (45 min) and the empty

testing chamber (5 min) for 3 d. The testing chamber was an opaque plastic chamber (61 × 42 × 37 cm) with regular rodent bedding. On testing day, the animals were set into the testing chamber for 1 min to rehabituate. Then two identical objects were placed into the testing chamber, and the rat was allowed to explore the objects for 15 min ("familiarization"). After a 3 h delay, the rat was replaced into the testing chamber again with one object identical to one used in the familiarization phase and a new object ("testing"). The rats were given 15 min to explore the familiar and new objects during the testing phase. The familiarization and testing phases were filmed with a digital video camera for off-line analysis. The analysis was done using the software developed by Robert E. Clark (University of California, San Diego, La Jolla, CA) using a hand-held game controller (Clark et al., 2000). The complete exploration time during the familiarization was scored. During the testing phase, the first 30 s of cumulative exploration time was scored. Two main criteria had to be fulfilled to be scored as exploratory behavior: (1) the animal's nose had to point toward the object not farther away than one rat head's length, and (2) there had to be a movement of the whiskers. The testing chamber and used objects were washed with 70% ethanol before the next rat was tested. All of the objects used were made of plastic and did not differ in overall size but differed in shape and color. Objects and positions in the testing chamber were systematically counterbalanced between groups.

Recording of the EEG and EMG. EEG/EMG recordings were performed as described previously (Beuckmann et al., 2004). Female Fisher 344 rats (180–200 g; $n = 3$ per group) were anesthetized (50 mg/kg ketamine, 5 mg/kg xylazine, and 1 mg/kg acepromazine, i.p.), held in a stereotaxic apparatus, and surgically implanted under sterile conditions with a miniaturized prefabricated block of recording electrodes. The electrode block was lowered stereotaxically until the electrodes just penetrated the skull and just touched the dura. This depth was critical to ensure that the lower end of the electrode made electrical contact with the dura but did not penetrate it. The electrode block was then affixed to the skull using a glass ionomer dental cement (Ketac Cem, ESPE; 3M, St. Paul, MN). EEG signals were recorded unilaterally from a fronto-occipital electrode pair, positioned 1.5 mm rostral and 1.45 mm laterally from bregma, and 6.1 mm caudal and 1.45 mm lateral from bregma. EMG signals were recorded concurrently from two flexible wires, insulated except at the tips, and implanted bilaterally by blunt dissection into the nuchal musculature. All rats recovered from the surgery and were habituated to the recording conditions for 3 weeks before recording commenced. Throughout the recording, the rats were tethered via a lightweight cable that was attached to a counterbalanced arm (SMCLA; Instech Laboratories, Plymouth Meeting, PA) mounted to the side of a standard shoebox cage, with the top cut away. EEG/EMG signals were recorded under controlled conditions (12 h light/dark cycle; 24 ± 1°C) for 3 consecutive days. Signals were digitized at 250 Hz, recorded to hard disk, and subsequently archived to optical media for off-line analysis. Concurrently with EEG/EMG recording, the behavior of the rats was videotaped for 4 h. Using customized display software, each 24 h EEG record was visually screened in 20 s epochs for seizure epochs, the timing and duration of each seizure was noted, and comparison was made against the behavior of the rat from the synchronized video record during the initial period. The display was in terms of 20 s epochs. Seizures were characterized as a spike-wave pattern on the EEG, usually accompanied by atonic periods or sustained rhythmic contractions on the EMG. Repetitive spike-wave patterns were frequently observed, sometimes accompanied by rhythmic slow activity. Fast waves of increasing amplitude and decreasing frequency could also be seen. Subclinical seizures were typically evident on the EEG record as a lower-amplitude abnormal wave pattern without change to the EMG. Each seizure lasting for 2 s or more was noted, and those that occurred within 5 s of each other were considered the same seizure. Analysis was in terms of the total number and of the mean duration of seizures during the 12 h dark and light periods.

Statistics. All statistical analyses were performed using Statview 5.0.1 (SAS Institute, Cary, NC). For all comparisons, ANOVA was performed followed by Fisher's *post hoc* test, when appropriate. Differences were considered statistically significant at $p < 0.05$.

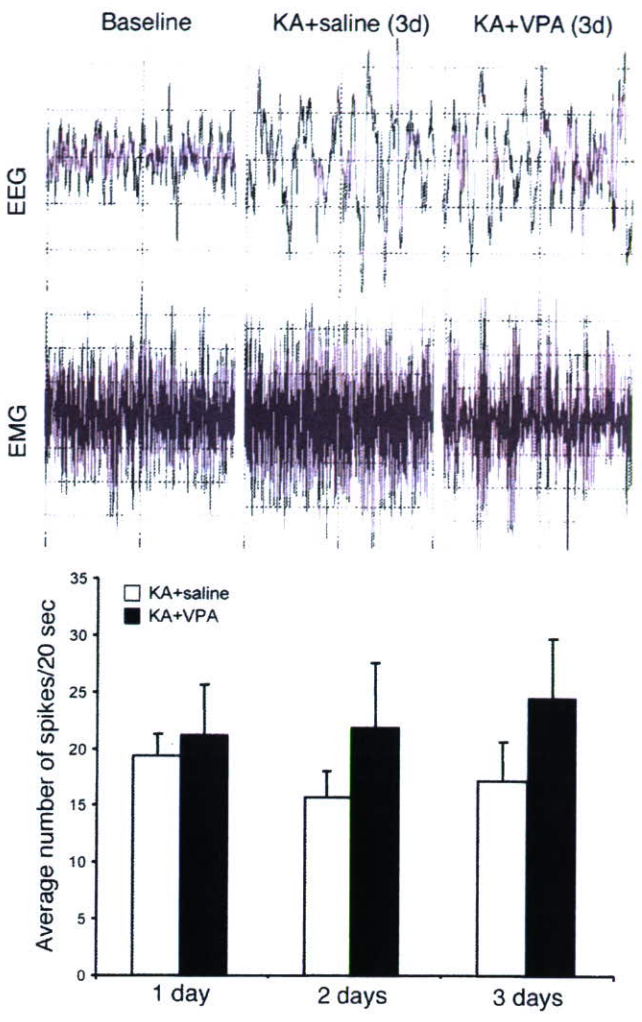

Figure 1. Representative examples of EEG monitoring at baseline and spike-wave activity characteristic of seizures in KA-treated animals receiving saline or VPA injections after 3 d. Quantification of the average number of spikes per 20 s time period between VPA- and saline-treated seizure animals at 1, 2, and 3 d, showing no significant difference between the two groups.

Results

KA-induced subclinical seizures persist with VPA treatment

We used KA to induce SE in Fisher 344 rats, because they show relatively little variance in their response to KA (Golden et al., 1995). Seizures could be detected behaviorally within 1 h after KA injection and lasted for at least 2–3 h. To examine whether VPA affected seizure activity, we injected rats with either VPA or saline 5 h after initial seizure onset and started EEG monitoring. Both groups showed similar, pronounced spike-wave epileptiform discharges consistent with behavioral seizures during the first 24 h (Fig. 1). Even after overt behavioral seizures subsided after the first day, both seizure groups still showed spike wave activity characteristic of subclinical seizures for up to 3 d of EEG/EMG monitoring. Thus, VPA treatment in seizure animals did not significantly affect seizure strength or frequency in the first 3 d after KA injection compared with untreated seizure control animals.

VPA inhibits seizure-induced neurogenesis in the adult dentate GCL

To examine the potential effects of VPA on seizure-induced neurogenesis, we used the thymidine analog BrdU to label dividing

cells and their progeny. The animals were separated into two groups, an early group receiving 7 d of BrdU injections and killed 1 d after the last BrdU injection (proliferation group) and a late group receiving 7 d of BrdU injections and killed 4 weeks later (survival group). Consistent with previous reports (Bengzon et al., 1997; Parent et al., 1997; Scott et al., 1998), seizure activity induced a strong increase in BrdU-positive cells in the DG of animals in the early group compared with animals injected with saline or VPA only (Fig. 2*A–E*) ($p < 0.01$). Animals receiving daily VPA injections after KA-induced seizures displayed reduced levels of BrdU-positive cells compared with seizure animals without VPA (Fig. 2*A–E*).

To determine the phenotype of dividing cells mediating the KA-induced increase in cell proliferation in the presence or absence of VPA, we analyzed proliferating progenitors (using Ki67 as a marker of cycling cells) (Gerdes et al., 1983; Kee et al., 2002) for their coexpression of DCX, a marker for dividing neuroblasts and immature neurons (Brown et al., 2003; Couillard-Despres et al., 2005; Jessberger et al., 2005) by confocal microscopy. The number of Ki67-positive colabeling with DCX increased in animals treated with KA (Fig. 2*K,L*) ($p < 0.01$). However, KA-injected animals treated with VPA did not display an increase in DCX–Ki67 double-positive cells and showed levels similar to those in control and VPA-treated only animals (Fig. 2*L*).

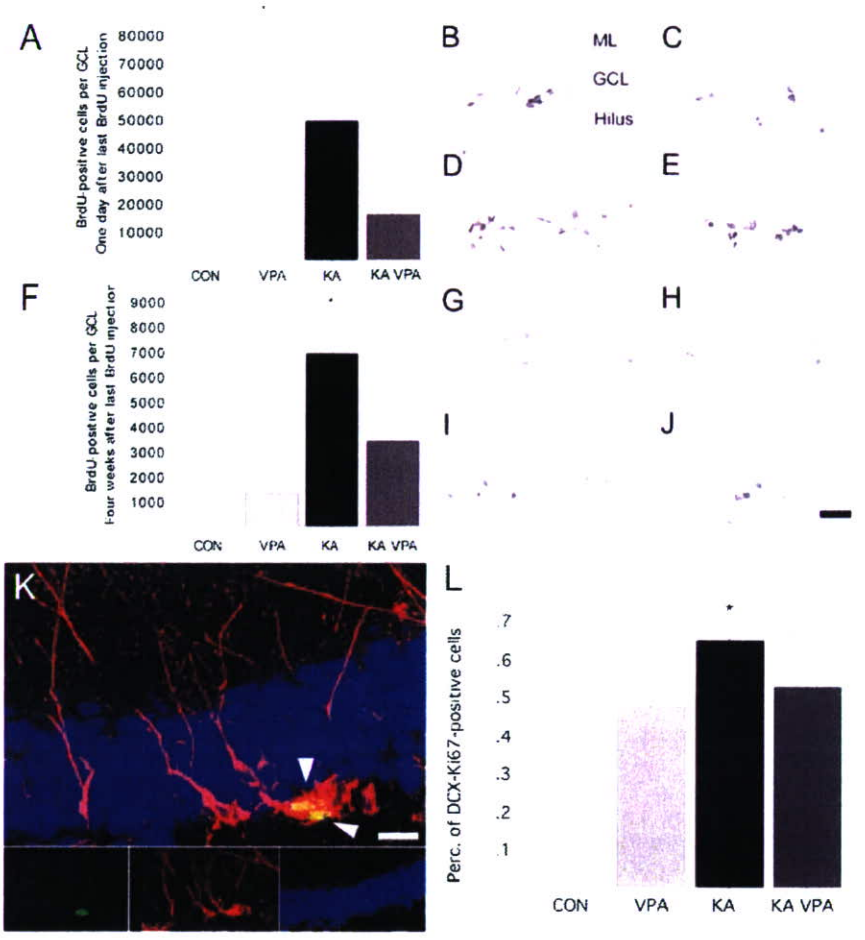

Figure 2. VPA treatment blocks seizure-induced neurogenesis and prevents aberrant DCX-expressing progenitor cell activation. ***A–E***, Number of BrdU-positive cells 1 d after the last BrdU injection, indicative of proliferative activity after SE (***A***). Representative BrdU staining of saline (***B***), VPA-treated (***C***), KA-injected (***D***), and KA-injected plus VPA-treated (***E***) animals killed 1 d after last BrdU injection. ***F–J***, Number of BrdU-positive cells 4 weeks after the last BrdU injection, indicative of stable cell genesis after SE (***F***). Representative BrdU staining of saline (***G***), VPA-treated (***H***), KA-injected (***I***), and KA-injected plus VPA-treated (***J***) animals killed 4 weeks after last BrdU injection. ***K***, Example of two DCX (red)/Ki-67 (green) colabeled cells (arrowheads) in the subgranular zone (blue, NeuN) 8 d after SE. ***L***, The percentage of DCX/Ki-67 colabeled cells is increased 8 d after SE compared with controls. VPA treatment prevents aberrant DCX-positive progenitor cell activation. Scale bars: (in ***J***) ***B–J***, 100 μm; ***K***, 20 μm. $^*p < 0.01$.

We next examined the number of BrdU-labeled cells in the DG of animals in the survival group. Reflecting the strong increase in proliferation soon after SE, there was a significant increase in the number of BrdU-positive cells in KA-treated animals. Strikingly, the seizure-induced increase in net neurogenesis was significantly reduced with VPA treatment (Fig. 2*F–J*). To identify the phenotype of BrdU-labeled cells 4 weeks after the last BrdU injection, we determined the percentage of cells that were positive for BrdU and positive for NeuN, a marker of mature neurons or S100β, a Ca^{2+}-binding protein expressed by astrocytes. We did not find any significant differences in relative neuronal or glial differentiation of newborn cells (data not shown). However, the absolute number of BrdU–NeuN double-positive cells in the KA-treated group was substantially increased compared with that in control and VPA-alone animals (Fig. 3*A–C*). Notably, seizure animals that had received VPA injections showed numbers of newborn neurons that were comparable with those in control animals, showing that VPA potently inhibited seizure-induced neurogenesis in the adult hippocampus.

VPA normalizes the morphology of newly generated dentate granule cells after seizures

One of the characteristic changes seen after SE is the presence of hilar basal dendrites arising from granule cells that fail to retract and extend their processes deep into the hilus (Buckmaster and Dudek, 1999; Dashtipour et al., 2003; Shapiro and Ribak, 2006). The presence of these hilar basal dendrites on dentate granule cells as well as ectopic hilar granule cells after seizures could lead to a recurrent excitatory circuitry (Ribak et al., 2000; Scharfman et al., 2000). Therefore, we analyzed the extent of DCX-positive basal dendrites reaching into the hilus. Confirming previous results (Dashtipour et al., 2003; Shapiro and Ribak, 2006), we found a significant increase in the length and number of dendritic processes reaching into the hilus 8 d after KA-induced seizures compared with controls (Fig. 3*E*). VPA treatment of seizure animals almost completely prevented the formation of hilar basal dendrites and normalized the morphology of newborn granule cells similar to controls (Fig. 3*E*).

VPA inhibits seizure-mediated neurogenesis by regulating changes in gene expression

The observation that there was a decrease in the number of newborn neurons and normalized morphology after seizures with VPA treatment led us to investigate how VPA acts to block the detrimental effects of seizure-induced neurogenesis. The effect of

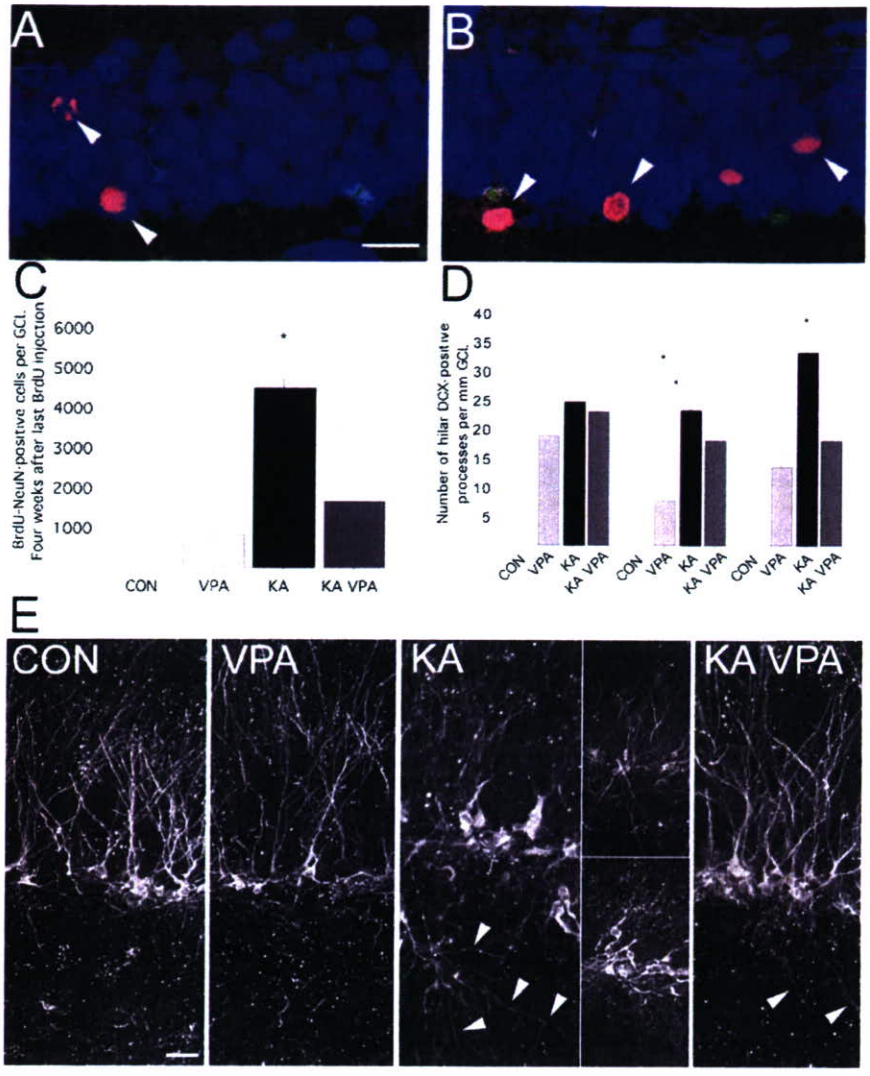

Figure 3. VPA treatment abates the number of seizure-generated neurons and decreases the formation of hilar basal dendrites. ***A–C***, Compared with control animals (***A***), the number of new neurons (arrowheads) 4 weeks after the last BrdU injection is dramatically increased after KA injection (***B***; red, BrdU; blue, NeuN; green, S100β). VPA treatment significantly reduced the number of new neurons after SE (***C***). ***D***, ***E***, VPA treatment inhibited the formation of basal dendrites reaching into the polymorphic cell layer (***D***). Representative examples of DCX-immunoreactive cells in saline (CON), VPA-treated (VPA), KA-injected (KA), and KA-injected plus VPA-treated (KA VPA) animals killed 8 d after SE (***E***). Arrowheads point toward hilar basal dendrites. Scale bars: ***A***, ***E***, 20 μm. $^*p < 0.01$.

KA-induced seizures on NRSF transcripts has been studied in the adult brain (Palm et al., 1998). The researchers found increased expression of NRSF in granular neurons of the DG 4 h after KA treatment and increased expression in the pyramidal layers CA1–CA4 24 h after KA treatment. In our experiments, a time course RT-PCR after KA treatment was performed (Fig. 4*A*). Indeed, NRSF mRNA levels were significantly increased in both the DG and CA3 as early as 6 h after KA injection and remained elevated throughout the course of the experiment (Fig. 4*A*). In other experiments, NRSF levels returned to baseline at 3 d after KA treatment, suggesting that there may be a critical period initially after SE that NRSF regulation of direct downstream target genes is occurring. NRSF protein levels appeared relatively unchanged in control and KA-treated animals at various time points (3 h to 3 d), although there may be slightly increased NRSF protein levels at the 1 d time point with KA treatment in both DG and CA3 (Fig. 4*B*).

KA-induced seizures have been shown to upregulate the expression of some NRSF target genes, such as BDNF (Zafra et al., 1990; Tongiorgi et al., 2004) and NaCh II (Gastaldi et al., 1997), and downregulate the expression of other genes, such as GluR2 (Grooms et al., 2000; Sanchez et al., 2001). We found that there are gene-specific differences among various NRSF target genes (i.e., GluR2, BDNF, synapsin I) with respect to their upregulation or downregulation after KA in the DG at 3 and 24 h (Fig. 4*C*). We also observed GluR2 protein levels were down by 3 d with KA treatment in both DG and CA3, which has been suggested previously to be one of the critical genes downregulated after seizures (Fig. 4*B*) (Pollard et al., 1993; Friedman et al., 1994). Interestingly, animals receiving both KA and either VPA (K/V) or TSA (K/T) displayed high levels of NRSF-regulated gene expression as early as 3 h (as for BDNF and synapsin I) and, in some cases, up to 24 h (as for BDNF). In the case of GluR2, there was downregulation of the message after KA induction by 24 h, which was prevented with VPA or TSA treatment (Fig. 4*C*). This finding is consistent with results from Huang et al. (2002), who demonstrated that TSA prevented the downregulation of GluR2 in CA3 after pilocarpine-induced seizures (Huang et al., 2002). As for BDNF (at 3 and 24 h) and synapsin I (at 3 h), VPA or TSA treatment in KA-injected animals kept the mRNA levels high; however, the level of synapsin I dropped back down to baseline by 24 h. These results suggest that NRSF and a subset of NRSF target genes may be preferentially dysregulated after KA-induced seizures and that VPA, through HDAC inhibition, may function to normalize these aberrant changes in gene expression.

In the above experiments, animals were first pretreated with VPA or TSA for 1 h before seizure induction to maximize the levels of HDAC inhibitors during SE (as described previously by Huang et al., 2002). In a follow-up study, we treated seizure rats with VPA (K/V), TSA (K/T), or valpromide (K/M) 5 h after onset of SE, which is identical to the paradigm for the neurogenesis and behavioral studies with the addition of a second HDAC inhibitor (Fig. 4*D*). Similar to the pretreatment scheme, VPA and TSA (although to a lesser extent) prevented the KA-induced downregulation of GluR2. Interestingly, the antiepileptic valpromide (K/V), which is an amide analog of VPA but is not an HDAC inhibitor (Gottlicher et al., 2001), does not block the downregulation of GluR2 after KA treatment. Together, these data suggest that VPA blocks seizure-induced neurogenesis via inhibiting HDACs, possibly through modulation of NRSF activity and neuronal target genes.